AD-A010 194

CUMULUS CLOUD ENERGETICS AS REVEALED IN A NUMERICAL
MODEL OF CLOUD DYNAMICS

L. Randall Koenig, et al

RAND Corporation

REPORT DOCUMENTATION PAGE		READ INSTRUCTIONS BEFORE COMPLETING FORM
1. REPORT NUMBER R-1613-ARPA	2. GOVT ACCESSION NO.	3. RECIPIENT'S CATALOG NUMBER AD-A010 194
4. TITLE (and Subtitle) Cumulus Cloud Energetics as Revealed in a Numerical Model of Cloud Dynamics		5. TYPE OF REPORT & PERIOD COVERED Interim
		6. PERFORMING ORG. REPORT NUMBER
7. AUTHOR(s) L. Randall Koenig and Francis W. Murray		8. CONTRACT OR GRANT NUMBER(s) DAHC15-73-C-0181
9. PERFORMING ORGANIZATION NAME AND ADDRESS The Rand Corporation 1700 Main Street Santa Monica, Ca. 90406		10. PROGRAM ELEMENT, PROJECT, TASK AREA & WORK UNIT NUMBERS
11. CONTROLLING OFFICE NAME AND ADDRESS Defense Advanced Research Projects Agency Department of Defense Arlington, Va. 22209		12. REPORT DATE April 1975
		13. NUMBER OF PAGES 94
14. MONITORING AGENCY NAME & ADDRESS(if different from Controlling Office)		15. SECURITY CLASS. (of this report) UNCLASSIFIED
		15a. DECLASSIFICATION/DOWNGRADING SCHEDULE

16. DISTRIBUTION STATEMENT (of this Report)

Approved for Public Release; Distribution Unlimited

17. DISTRIBUTION STATEMENT (of the abstract entered in Block 20, if different from Report)

No restrictions

18. SUPPLEMENTARY NOTES

19. KEY WORDS (Continue on reverse side if necessary and identify by block number)

Cloud Physics
Atmospheric Electricity
Cumulus Clouds
Climatology

20. ABSTRACT (Continue on reverse side if necessary and identify by block number)

see reverse side

DD FORM 1473 EDITION OF 1 NOV 65 IS OBSOLETE

R-1613-ARPA
April 1975

Cumulus Cloud Energetics as Revealed in a Numerical Model of Cloud Dynamics

L. Randall Koenig and Francis W. Murray

A Report prepared for

DEFENSE ADVANCED RESEARCH PROJECTS AGENCY

Rand
SANTA MONICA, CA. 90406

ii

PREFACE

It has long been suspected that cumulus clouds are major factors in the vertical transport of energy, mass, and momentum in the atmosphere, particularly in the tropical latitudes. If they are, those factors must be taken into consideration in designing simulation models of larger-scale atmospheric phenomena, especially those depicting the general circulation of the entire world-wide atmosphere. Typically, planetary-scale models use computation grid intervals too large to permit the horizontal resolution of cumulus activity; therefore, the cloud itself cannot be directly included in the set of governing equations. But the cumulative effect of all clouds within a grid cell must be taken into account if the larger-scale model is to properly simulate the global atmospheric dynamics and energetics. For that reason there has been a considerable effort to develop parametric schemes to account for cumulus activity, using approaches that have included both field measurements and theoretical arguments.

A useful parametric scheme would be one that in some way realistically simulated the integrated effect of the whole set of convective elements on the large-scale circulation, temperature, and other variables. It must not require as input any information with higher resolution in space or time than the standard resolution of the large-scale model, nor may its output be of such high resolution. If the parameterization were simple enough, it could be incorporated into the large-scale equations and solved simultaneously with them. More probably, it would be too complex for that, and so after the large-scale computations were made, the parameterization would take these preliminary results as input data, would determine the changes to the variables due to convection, and would feed the revised conditions back to the large-scale model.

A reasonable way to go about developing such a parameterization would be to determine first in some detail how an individual convection element affects its environment, and then to generalize from this knowledge. The present work represents only the first step in this procedure.

In this work the transformation from one kind of energy (e.g., latent enthalpy, kinetic energy) to another and the rearrangement in time and space of different kinds of energy as a result of cumulus convection are analyzed by the use of a numerical model of cumulus dynamics. These kinds of data provide the basic information necessary to develop parametric schemes for use in the larger-scale models.

This report is one of a series on the dynamics of climate, a Rand project sponsored by the Defense Advanced Research Projects Agency. A large part of the work, however, was supported by the Navy Environmental Prediction Research Facility and by Corporate funds set aside for Rand-sponsored research. It is directly related to Rand's continuing interest in smaller-scale atmospheric phenomena. For other related work, see the following Rand publications:

R-852-ARPA, *Numerical Experiments on the Relation Between Microphysics and Dynamics in Cumulus Convection*, F. W. Murray and L. R. Koenig, September 1971.

R-877-ARPA, *A Documentation of the Mintz-Arakawa Two-Level Atmospheric General Circulation Model*, W. L. Gates, E. S. Batten, A. B. Kahle, and A. B. Nelson, December 1971.

R-1005-ARPA, *The January Global Climate Simulated by the Two-Level Mintz-Arakawa Model: A Comparison with Observation*, W. L. Gates, November 1972.

R-1415-ARPA, *Some Predicted Climatic Effects of a Simulated Sahara Lake*, R. R. Rapp and M. Warshaw, March 1974.

R-1429-ARPA, *A Numerical Experiment on the Effects of Regional Atmospheric Pollution on Global Climate*, L. R. Koenig, June 1974.

SUMMARY

Using a numerical model previously designed to simulate atmospheric convection, this study investigates the effects of cumulus clouds on the temporal and spatial characteristics of atmospheric energy content.

The forms of energy investigated are latent enthalpy, thermal enthalpy of water vapor, thermal enthalpy of dry air, thermal enthalpy of airborne liquid and of rain that has fallen, potential energy, and kinetic energy. Work done by the pressure force is excluded because the volume of the domain is constant. There is no change of pressure at the upper boundary, and only very small changes at the lower and lateral boundaries.

Changes in energy content of the cloud environment and the flux of energy are shown as functions of height and radial distance from the cloud axis. These changes are also summed vertically and horizontally over the domain to show the horizontal and vertical rearrangement of energy. The influence of the cloud is largely confined to distances within a few cloud radii.

The relative importance of different energy forms is a function of position with respect to the cloud. Energy related to the presence of water vapor (latent plus thermal enthalpy of water vapor) has been found to account for the majority of the change in energy in the vicinity of the cloud. In the outer region changes in enthalpy of water vapor are counterbalanced by changes in the enthalpy of dry air, but potential energy change dominates.

The total energy used in attempting to decrease conditional instability in the atmosphere is given by the total amount of energy produced by the condensate formed--regardless of whether or not it falls as rain. Clouds of differing sizes will cause differing amounts of energy rearrangement. The simulated "clouds" used in this work resemble in size the cells in some of the larger natural clouds (but not the largest of them) observed in the vicinity of the station at which the sounding was taken. Thus their convective activity should represent reasonably well that of the real cloud cells. The amount by which

the action of the computed cell reduces the potential instability of the atmosphere in its neighborhood is 0.5 percent of that required to establish neutral stability. This datum, together with reasonable assumptions about the number and frequency of occurrence of such cells, leads to an estimated relaxation time of convection of approximately ten hours. That is, ten hours is required for the departure from neutral stability to be reduced to $1/e$ of its initial value.

ACKNOWLEDGMENTS

CONTENTS

FIGURES

SYMBOLS

VECTOR VARIABLES

$\underset{\sim}{k}$	unit vertical vector
$\underset{\sim}{v}$	wind velocity

SCALAR VARIABLES

A	horizontal area
c	specific heat capacity
D	mesh length
E	energy within a volume element
F	vertical flux of energy
g	acceleration due to gravity
h	specific energy
$h^\star$	dry-air specific energy
L	latent heat of condensation
m	mass of a parcel
n	number of time-steps
p	pressure
q	mixing ratio
R	depth of rain
r	radial distance
T	temperature
u	horizontal wind component
V	volume
w	vertical wind component
Z	depth or height
α	arbitrary constant or variable independent of time
η	energy density
ν	eddy diffusion coefficient
ρ	density
τ	a given time
ξ	product of specific energy and a given horizontal area

SCALAR VARIABLES (continued)

ϕ	dummy variable
θ	dummy variable

COORDINATES AND INDICES

i	horizontal index
I	maximum value of horizontal index
k	vertical index
K	maximum value of vertical index
t	time coordinate
x,y,z	space coordinates

SUBSCRIPTS

a	dry air
E	enthalpy
G	gross or total energy
i	horizontal index
K	kinetic energy
k	vertical index
L	latent enthalpy
ℓ	condensed water
m	mean (reference) value
P	potential energy
p	at constant pressure
R	rain
S	static energy
T	thermal enthalpy
t	time index
v	water vapor
z	dependent on height only
0	initial time
τ	a given time
ϕ	dummy variable
θ	dummy variable

SPECIAL SYMBOLS

(φ is a dummy variable)

$\bar{\phi}$	reference value	Eq. (2-10)
ϕ'	departure from reference value	Eq. (2-10)
$\tilde{\phi}$	time average	Eq. (3-26)
ϕ''	departure from time average	Eq. (3-25)
$\bar{\phi}^S$	horizontal space average	Eq. (3-31)
$\phi*$	departure from horizontal space average	Eq. (3-34)
$\bar{\phi}^A$	area-weighted horizontal space average	Eq. (3-32)
$\Delta\phi$	change over specified time interval	Eq. (3-14)
$\delta\phi$	change over single time-step	Eq. (3-11)
$\langle\phi\rangle$	summation by slabs	Eq. (3-6)
$[\phi]$	summation by tubes	Eq. (3-7)
$\{\phi\}$	summation over the domain	Eq. (3-8)
$\mathscr{D}(F_\phi)$	vertical divergence	Eq. (3-41)

1. INTRODUCTION

Cumulus convection is known to play an important role in the transformation and rearrangement of energy in the atmosphere. As used here, "transformation" means the change of one type of energy to another (e.g., potential energy to kinetic energy), whereas "rearrangement" includes both changes of that type and transport from one location to another. The conceptually simple transformation of latent heat of condensation to sensible heat upon the condensation of water vapor grossly oversimplifies the true cloud-environment relationship. In actuality, the release of latent heat causes the generation of kinetic energy, which in turn results in the vertical and horizontal advection of mass and consequently of enthalpy and potential energy. There are then further transformations among the various types of energy as a function of space and time. Presumably, these transformations and rearrangements act to reduce the potential instability of the atmosphere. One of our problems is to find out how this is accomplished.

Although the amount of energy involved in the life cycle of a single convective cell is negligible by comparison with the energy of the larger organized circulations, the cumulative effect of many such cells has a profound influence on these larger circulations. Models of the general circulation or even mesoscale models cannot resolve convective cells, and so they must parameterize the convective activity as a subgrid-scale effect. Such a parameterization must realistically treat the cumulative effect of an ensemble of convective cells on atmospheric energetics; consequently, it should be based on the knowledge of the energetics of a single cell.

Recognition of the complexity and importance of cloud energetics has led to attempts to measure in the field those factors that describe the relationship between a cloud and its environment (e.g., Braham, 1952), and to a lesser degree to use theoretical models (e.g., Schlesinger, 1972) to analyze the cloud-environment interactions in terms of energy. The present study falls in the latter category.

This study makes use of a numerical model designed to simulate the life cycle of an individual cumulus cell (Murray and Koenig, 1972). The cloud model was not developed for the study of energetics; however, it produces fields of motion, temperature, pressure, humidity, and liquid water content at frequent time intervals, which makes it possible to compute the content of energy as a function of time and space. Hence, the output of the existing cloud model was used as the input for the present study of energetics.

Briefly, the cloud model effects the numerical solution of a set of equations including the equations of motion, the equations of con-servation of mass of air and of water substance, the first law of thermodynamics, the equation of state, and several equations describ-ing microphysical processes related to condensation, evaporation, drop coalescence, and fallout of rain. The Boussinesq approximation (Spiegel and Veronis, 1960) is used to simplify the hydrodynamical and thermo-dynamical equations, and the parameterization of Kessler (1969) is used for the microphysics. The solution is carried out in a vertical plane through an axis about which horizontal symmetry is assumed. Initially, the atmosphere is without liquid water, is horizontally homogeneous, and is at rest. Convection is started by the introduction of a small per-turbation of buoyancy or of momentum. Although the finite-difference scheme was not designed to conserve total energy, considerable care was taken to conserve the total mass of water substance, which consists of vapor, liquid drops, and rain that has fallen to the ground. Since water substance is involved in much of the cloud energetics, this fea-ture contributes strongly toward conservation of total energy.

The programs designed for the present study read the values of the meteorological variables computed by the cloud program and use them to compute a number of other quantities. Among these are specific energy of each type at each grid point and specified time, changes in these values from time zero up to the specified time, horizontal and vertical summations, and vertical fluxes.

Since one of the objectives is to relate cumulus-scale convection to circulations of mesoscale through planetary scale, some attention must be paid to problems of resolution. Atmospheric circulations of

horizontal scale larger than about 100 km are anisotropic in that their motions are quasi-horizontal. As has been mentioned, cumulus convection is completely nonresolvable in the horizontal on these larger scales. Their vertical and time scales, however, are such that cumulus convection can be crudely resolved. That is, vertical transports on the cumulus scale can work to relieve instabilities in the larger scales, and the length of time required for a cumulus cell to go through its life cycle is comparable to the appropriate time step for the larger scales. Hence, this study emphasizes average vertical fluxes and changes that occur from the time of inception of the convective cell until the conclusion of convection.

The term "cloud" is frequently used in this work to designate the airborne condensate simulated by numerical computation. Given that the model simulates the initiation, development, and decay of a convective element through one cycle of vertical drafts, the term "cloud tower" may more correctly describe the simulated entity, since in nature a cumulus cloud usually consists of more than one cell or tower. The characteristics of a "cell" simulated herein are rather similar to those of a representative thunderstorm cell as described by Brahan (1952).

II. CUMULUS ENERGETICS

ENERGY CATEGORIES

The energy content of a parcel of cloudy air may be subdivided into various categories:

1. Kinetic energy
2. Static energy
   a. Potential energy
   b. Enthalpy
      (1) Thermal enthalpy
      (2) Latent enthalpy

The terms "thermal enthalpy" and "latent enthalpy" are used by van Mieghem (1973). Meteorologists ordinarily use the terms "sensible heat" and "latent heat" for these properties. Thermal enthalpy is related to the heat capacity of the substance involved, and latent enthalpy is the energy related to a change of phase.

In this report the adjective "specific" applied to any category of energy associated with a substance will indicate the energy per unit mass of that substance. Let m_ϕ be the mass of substance ϕ contained within a parcel of cloudy air, where "ϕ" may be replaced by "a" for dry air, "v" for water vapor, or "ℓ" for condensed water. (See list of symbols above.) The mixing ratio of substance ϕ is defined as

$$q_\phi = \frac{m_\phi}{m_a} \qquad (2\text{-}1)$$

If h_ϕ is the specific energy related to substance ϕ, then

$$h^*_\phi = q_\phi h_\phi \qquad (2\text{-}2)$$

represents the energy of that substance per unit mass of dry air; it will be designated the "dry-air specific energy." Let the various

categories of energy be designated by subscripts, as follows:

h_G gross or total energy

h_K kinetic energy

h_S static energy

h_P potential energy

h_E enthalpy

h_T thermal enthalpy

h_L latent enthalpy

These subscripts may also be combined with the subscripts a, v, and ℓ to denote the substance involved. If neither a, v, nor ℓ is used, the symbol refers to cloudy air.

Energy expressed in the form of (2-2), being referred to the same unit mass for all categories, is additive. Hence

$$h^*_G = h^*_K + h^*_S \qquad (2\text{-}3)$$

$$h^*_S = h^*_P + h^*_E \qquad (2\text{-}4)$$

$$h^*_E = h^*_T + h^*_L \qquad (2\text{-}5)$$

$$h^*_E = h^*_{Ea} + h^*_{Ev} + h^*_{E\ell} \qquad (2\text{-}6)$$

$$h^*_T = h^*_{Ta} + h^*_{Tv} + h^*_{T\ell} \qquad (2\text{-}7)$$

Since all three components of cloudy air share the same height, and except for fallout of rain, the same velocity, the potential and kinetic energies are not broken down by substance. The enthalpy of each substance, however, is computed separately.

ENERGY EQUATION FOR A PARCEL OF CLOUDY AIR IN MOTION

The cloud model on which the present study is based is formulated in terms of the Boussinesq approximation as set forth by Spiegel and Veronis (1960), but with modifications to allow for the presence of water vapor and condensed water and to make it more applicable to moderately deep convection. Spiegel and Veronis divide all variables of state into three parts: a mean (constant) part, a part dependent only on height at initial time in the absence of motion, and a part related to motion. Thus, for density,

$$\rho = \rho_m + \rho_z(z) + \rho'(x,\ y,\ z,\ t) \tag{2-8}$$

The equation of motion then would be

$$\frac{d\underset{\sim}{v}}{dt} = -\frac{1}{\rho_m} \nabla p' - g \frac{\rho'}{\rho_m} \underset{\sim}{k} + \nu \nabla^2 \underset{\sim}{v} \tag{2-9}$$

where $\underset{\sim}{v}$ is the velocity (having horizontal component u and vertical component w), and the other symbols are as defined in the list above.

In the less restrictive anelastic equations of Ogura and Phillips (1962), the reference atmosphere is isentropic, and the variables of state are divided into only two parts:

$$\rho = \overline{\rho}(z) \cdot \rho'(x,\ y,\ z,\ t) \tag{2-10}$$

In the present context, ρ represents the density of cloudy air; hence

$$\rho = \rho_a + \rho_v + \rho_\ell = \rho_a(q_a + q_v + q_\ell) \tag{2-11}$$

where ρ_ℓ is construed as a "bulk density." The symbol q_a has been re-tained here and elsewhere for symmetry and clarity, even though $q_a \equiv 1$. The equation of motion can then be written as

$$\frac{d\underset{\sim}{v}}{dt} = -\frac{1}{\rho} \nabla p' - g \frac{\rho'}{\rho} \underset{\sim}{k} + \nu \nabla^2 \underset{\sim}{v} \tag{2-12}$$

The advantage of (2-12) over (2-9) is its better capability for deep convection. Also, in the study of energetics the use of $\bar{\rho}$ gives better results than does the use of ρ_m. The cloud model used herein has elements of both systems in it, but (2-12) will be used to develop the energy equation. If scalar multiplication by $\underset{\sim}{v}$ is performed on (2-12) and it is noted that $\underset{\sim}{v} \cdot \underset{\sim}{k} = w = dz/dt$, there results

$$\frac{d}{dt}\left(\frac{\underset{\sim}{v}^2}{2}\right) + \frac{\rho'}{\rho} \frac{d}{dt}(gz) = -\frac{1}{\rho} \underset{\sim}{v} \cdot \nabla p' + \nu \underset{\sim}{v} \cdot \nabla^2 \underset{\sim}{v} \qquad (2-13)$$

Expansion of p in the manner of (2-10) permits the first term on the right-hand side of (2-13) to be written

$$-\frac{1}{\rho} \underset{\sim}{v} \cdot \nabla p' = -\frac{1}{\rho}(\underset{\sim}{v} \cdot \nabla p - \underset{\sim}{v} \cdot \nabla \bar{p}) = \frac{1}{\rho}\left(w \frac{d\bar{p}}{dz} - \underset{\sim}{v} \cdot \nabla p\right) \qquad (2-14)$$

Although hydrostatic balance does not generally hold in a convective situation, the reference atmosphere is at rest and therefore hydrostatic. Hence (2-14) becomes:

$$-\frac{1}{\rho} \underset{\sim}{v} \cdot \nabla p' = -\frac{1}{\rho}(wg\bar{\rho} + \underset{\sim}{v} \cdot \nabla p) = -\frac{d}{dt}(gz) - \frac{1}{\rho} \underset{\sim}{v} \cdot \nabla p \qquad (2-15)$$

Furthermore,

$$-\frac{1}{\rho} \underset{\sim}{v} \cdot \nabla p = \frac{1}{\rho} \frac{\partial p'}{\partial t} - \frac{1}{\rho} \frac{dp}{dt} \qquad (2-16)$$

Combining (2-13), (2-15), and (2-16),

$$\frac{d}{dt}\left(\frac{\underset{\sim}{v}^2}{2}\right) + \frac{\rho'}{\rho} \frac{d}{dt}(gz) = -\frac{d}{dt}(gz) - \frac{1}{\rho}\frac{dp}{dt} + \frac{1}{\rho}\frac{\partial p'}{\partial t} + \nu \underset{\sim}{v} \cdot \nabla^2 \underset{\sim}{v}$$

or

$$\frac{d}{dt}\left(\frac{v^2}{2}\right) + \frac{\overline{\rho} + \rho'}{\overline{\rho}} \frac{d}{dt} (gz) + \frac{1}{\rho} \frac{dp}{dt} = \frac{1}{\rho} \frac{\partial p'}{\partial t} + \nu \underset{\sim}{v} \cdot \nabla^2 \underset{\sim}{v} \qquad (2-17)$$

The terms on the left-hand side of (2-17) will be recognized respectively as the rate of change of kinetic energy, potential energy, and enthalpy (provided there are no external sources or sinks of heat, such as radiation). All refer to unit mass of cloudy air. The terms on the right-hand side represent the work performed on the parcel by the pressure force and the eddy viscosity force. Both are small.

Since the third term represents the rate of change of total enthalpy of a unit mass of cloudy air, it can be written dh_E/dt. It remains to evaluate h_E.

In accordance with (2-6) together with (2-1) and (2-2), the enthalpy of a parcel of cloudy air is

$$(m_a + m_v + m_\ell)h_E = m_a h_{Ea} + m_v h_{Ev} + m_\ell h_{E\ell} \qquad (2-18)$$

The mass of the air remains constant, and except for the fallout of rain, which for the time being will be neglected, the total mass of water substance remains constant. That is,

$$dm_v = -dm_\ell \qquad (2-19)$$

Hence, differentiation of (2-18) leads to

$$(m_a + m_v + m_\ell) \, dh_E = m_a \, dh_{Ea} + m_v \, dh_{Ev} + m_\ell \, dh_{E\ell}$$
$$+ (h_{Ev} - h_{E\ell}) \, dm_v \qquad (2-20)$$

Expanding (2-20) according to the chain rule of differentiation,

$$(m_a + m_v + m_\ell) \, dh_E = m_a \left(\frac{\partial h_{Ea}}{\partial T}\right) dT + m_a \left(\frac{\partial h_{Ea}}{\partial p}\right) dp$$

$$+ \, m_v \left(-\frac{\partial h_{Ev}}{\partial T}\right) dT + m_v \left(\frac{\partial h_{Ev}}{\partial p}\right) dp$$

$$+ \, m_\ell \left(-\frac{\partial h_{E\ell}}{\partial T}\right) dT + m_\ell \left(\frac{\partial h_{E\ell}}{\partial p}\right) dp$$

$$+ \, (h_{Ev} - h_{E\ell}) \, dm_v \qquad (2\text{-}21)$$

The changes in specific enthalpy at constant pressure are by definition the specific heat capacities:

$$c_{pa} = \left(\frac{\partial h_{Ea}}{\partial T}\right); \quad c_{pv} = \left(\frac{\partial h_{Ev}}{\partial T}\right); \quad c_\ell = \left(\frac{\partial h_{E\ell}}{\partial T}\right) \qquad (2\text{-}22)$$

The changes in specific enthalpy at constant temperature are zero, and the difference in specific enthalpy between the two phases is the latent heat of condensation:

$$L = h_{Ev} - h_{E\ell} \qquad (2\text{-}23)$$

Hence (2-21) becomes

$$(m_a + m_v + m_\ell) \, dh_E = m_a c_{pa} \, dT + m_v c_{pv} \, dT$$

$$+ \, m_\ell c_\ell \, dT + L \, dm_v \qquad (2\text{-}24)$$

or, after division by m_a,

$$dh^*_F = (q_a + q_v + q_\ell) \, dh_E = (q_a c_{pa} + q_v c_{pv} + q_\ell c_\ell) \, dT + L \, dq_v \qquad (2\text{-}25)$$

Following the method of Iribarne and Godson (1973), we can use (2-23) to transform (2-18) into

$$(m_a + m_v + m_\ell)h_E = m_a h_{Ea} + m_v L + (m_v + m_\ell)h_{E\ell} \qquad (2\text{-}26)$$

Differentiation of (2-26) in the fashion of (2-21), followed by division by m_a, yields

$$dh^*_E = (q_a + q_v + q_\ell) \, dh_E$$

$$= (q_a c_{pa} + (q_v + q_\ell)c_\ell) \, dT + L \, dq_v + q_v \, dL \qquad (2\text{-}27)$$

The two expressions for the dry-air specific enthalpy of a parcel of cloudy air, (2-25) and (2-27), are equivalent. Ordinarily, the variation of latent heat with temperature can be neglected in meteorology, but if that is done in integrating (2-27), the resulting expression for the dry-air specific enthalpy of water vapor is $q_v c_\ell T$, whereas the correct expression from the integration of (2-25) is $q_v c_{pv} T$. The former is too large by a factor of $c_\ell / c_{pv} = 4187/1846 = 2.27$. If (2-25) and (2-27) are equated, Kirchoff's equation results:

$$c_\ell - c_{pv} = -\frac{dL}{dT} \qquad (2\text{-}28)$$

In order to make (2-25) compatible with (2-17), the enthalpy must be expressed in terms of unit mass of cloudy air rather than of dry air. This can be accomplished by multiplying (2-25) by $\bar{\rho}_a / \bar{\rho}$ or alternatively by dividing (2-24) by $m_a + m_v + m_\ell$. In accordance with (2-11) and the conservation of mass of air and of total water substance,

$$\frac{\bar{\rho}_a}{\bar{\rho}} = \frac{1}{\bar{q}_a + \bar{q}_v + \bar{q}_\ell} = \frac{1}{q_a + q_v + q_\ell} = \frac{\rho_a}{\rho} \qquad (2\text{-}29)$$

Hence from (2-25)

$$dh_E = \frac{\bar{\rho}_a}{\bar{\rho}} (q_a c_{pa} + q_v c_{pv} + q_\ell c_\ell) \, dT + \frac{\bar{\rho}_a}{\bar{\rho}} L \, dq_v \qquad (2\text{-}30)$$

and since

$$dh_E = \frac{1}{\rho} \, dp \qquad (2-31)$$

it follows that (2-17) becomes

$$\frac{d}{dt}\left(\frac{v^2}{2}\right) + \frac{\rho}{\bar{\rho}} \frac{d}{dt} \, (gz) + \frac{\bar{\rho}_a}{\bar{\rho}} \, (q_a c_{pa} + q_v c_{pv} + q_\ell c_\ell) \frac{dT}{dt}$$

$$+ \frac{\bar{\rho}_a}{\bar{\rho}} \, L \, \frac{dq_v}{dt} = \frac{1}{\bar{\rho}} \frac{\partial p'}{\partial t} + \nu \underset{\sim}{v} \cdot \nabla^2 \underset{\sim}{v} \qquad (2-32)$$

The terms on the left-hand side of (2-32) represent the rate of change of four kinds of specific energy: kinetic energy, potential energy, thermal enthalpy, and latent enthalpy. Therefore, using (2-2) and (2-29)

$$h^*_K = (q_a + q_v + q_\ell)(u^2 + w^2)/2 \qquad (2-33)$$

$$h^*_P = (q_a + q_v + q_\ell) \frac{\rho}{\bar{\rho}} \, gz \qquad (2-34)$$

$$h^*_T = (q_a c_{pa} + q_v c_{pv} + q_\ell c_\ell)T \qquad (2-35)$$

$$h^*_{Ta} = q_a c_{pa} T \qquad (2-36)$$

$$h^*_{Tv} = q_v c_{pv} T \qquad (2-37)$$

$$h^*_{T\ell} = q_\ell c_\ell T \qquad (2-38)$$

$$h^*_L = q_v L \qquad (2-39)$$

The factor $\rho/\bar{\rho}$ in (2-34) is, in accordance with (2-29), equal to $\rho_a/\bar{\rho}_a$, which is very nearly unity, so it might well be neglected. As will be seen later, however, the nature of the Boussinesq approximation dictates that it should be retained.

All forms of energy shown in (2-17) with the exception of those related to local pressure change and eddy viscosity are defined by (2-33) through (2-39). In a Boussinesq system the local pressure change is small and is usually ignored. The cloud model computations confirm that it is extremely small, and since the highly implicit nature of the problem makes that computation less accurate than those of the other variables of state, the local pressure change term will not be further discussed. The eddy diffusion term presumably represents a conversion of kinetic energy to heat, but in a finite-difference solution it could represent a sink of energy through the cascade effect to larger wave numbers. In any case, the kinetic energy itself is very small, so the eddy diffusion is quite negligible.

ENERGY DENSITY

For purposes of summation, it is more convenient to refer energy to unit volume rather than to unit mass. This can be achieved by multiplying (2-32) by $\bar{\rho}$, resulting in

$$
\bar{\rho} \frac{d}{dt}\left(\frac{v^2}{2}\right) + \rho \frac{d}{dt}(gz) + \bar{\rho}_a(q_a c_{pa} + q_v c_{pv} + q_\ell c_\ell) \frac{dT}{dt}
$$

$$
+ \bar{\rho}_a L \frac{dq_v}{dt} = \frac{\partial p'}{\partial t} + \nu \bar{\rho} \underset{\sim}{v} \cdot \nabla^2 \underset{\sim}{v} \tag{2-40}
$$

Then, corresponding to the expressions for energy per unit mass of dry air found in (2-33) through (2-39), one may write the following expressions for energy per unit volume, or energy density, with the aid of (2-11) and (2-29):

$$
\eta_K = \bar{\rho}_a(q_a + q_v + q_\ell)(u^2 + v^2)/2 \tag{2-41}
$$

$$
\eta_P = \rho gz = \rho_a(q_a + q_v + q_\ell)gz \tag{2-42}
$$

$$
\eta_T = \bar{\rho}_a(q_a c_{pa} + q_v c_{pv} + q_\ell c_\ell)T \tag{2-43}
$$

$$\eta_{Ta} = \bar{\rho}_a q_a c_{pa} T \tag{2-44}$$

$$\eta_{Tv} = \bar{\rho}_a q_v c_{pv} T \tag{2-45}$$

$$\eta_{T\ell} = \bar{\rho}_a q_\ell c_\ell T \tag{2-46}$$

$$\eta_L = \bar{\rho}_a L q_v \tag{2-47}$$

III. COMPUTATIONAL METHODS

VOLUME ELEMENTS

The Rand cloud model (Murray and Koenig, 1972) as used in the present experiment is formulated in cylindrical coordinates and assumes axial symmetry. A grid of uniform mesh length D is constructed, with the horizontal index i running from 1 at the central axis to I at the lateral wall, and the vertical index k running from 1 at the top to K at the bottom. In the present experiment, D = 200 m, I = 31, and K = 45; hence, the computational domain is a cylinder of radius 6 km and height 9 km.

It is assumed that values for a grid point are representative of a volume element about the grid point delimited by vertical cylindrical and horizontal plane surfaces constructed midway between the given grid point and its closest neighbors. Thus, the volume element represented by grid point (i,k) has the horizontal area

$$
\left.
\begin{aligned}
A_1 &= \pi D^2/4 \\[2ex]
A_i &= \pi\left(r_i + \frac{D}{2}\right)^2 - \pi\left(r_i - \frac{D}{2}\right)^2 \\[1ex]
&= 2\pi r_i D; \quad 1 < i < I \\[2ex]
A_I &= \pi r_I^2 - \pi\left(r_I - \frac{D}{2}\right)^2 \\[1ex]
&= \pi D\left(r_I + \frac{D}{4}\right)
\end{aligned}
\right\}
\tag{3-1}
$$

and depth

$$
\left.
\begin{aligned}
Z_k &= D; \quad 1 < k < K \\[1ex]
Z_1 &= Z_K = D/2
\end{aligned}
\right\}
\tag{3-2}
$$

where r_i, the radial distance from the central axis, is given by

$$r_i = (i - 1)D \tag{3-3}$$

The volume of the element represented by grid point (i,k) is then

$$V_{i,k} = A_i Z_k \tag{3-4}$$

The special cases for $i = I$, $k = 1$, and $k = K$ are the result of assuming that the computational domain ends at rigid surfaces constructed through the grid points on the boundary rather than at a distance of $D/2$ beyond them. The choice of this boundary assumption was arbitrary.

SUMMATIONS

The total energy of any given type, θ, residing within the volume element represented by the grid point (i,k) is then

$$E_{\theta_{i,k}} = \theta_{i,k} V_{i,k} \tag{3-5}$$

where θ can be replaced with K for kinetic energy, P for potential energy, etc. These values, then, can be summed in various ways. In particular, three types of summation are used in the present work.

Let ϕ be any quantity defined at the grid points. Then the summation of ϕ by *slabs* (i.e., horizontally) will be denoted by angular brackets:

$$\langle \phi \rangle_k = \sum_{i=1}^{I} \phi_{i,k} \tag{3-6}$$

The summation of ϕ by *tubes* (i.e., vertically) will be denoted by square brackets:

$$[\phi]_i = \sum_{k=1}^{K} \phi_{i,k} \tag{3-7}$$

The summation over the entire domain will be denoted by braces:

$$\{\phi\} = \sum_{i=1}^{I} \sum_{k=1}^{K} \phi_{i,k} \tag{3-8}$$

It will be noted that summation over the domain is equivalent to successive summation by slabs and by tubes in either order; i.e.,

$$\{\phi\} = \langle [\phi]_i \rangle = [\langle \phi \rangle_k] \tag{3-9}$$

If the total mass of dry air in the closed computational domain is to be conserved, then it is necessary that

$$\{\rho_a V\} = \text{constant} \tag{3-10}$$

This is assured in the present model, which is based on the Boussinesq approximation, by substituting $\bar{\rho}_a$, a function of k only, for ρ_a. This substitution is fully consistent with the use of $\bar{\rho}_a$ in computing all energy densities except potential energy density; see equations (2-41) through (2-47). It imposes the restriction that the work of expansion is zero, which is consistent with the fixed volume of the domain and the fixed volume represented by each grid point.

ENTHALPY OF RAIN

During the operation of the cloud model, a part of the condensed liquid falls out as rain. This represents a certain amount of energy (thermal enthalpy) that is removed from the atmosphere.

If R_i is the depth of rain on the ground in millimeters over the area A_i, then $R_i A_i$ is the mass in kilograms of that amount of water, since the density of water is 10^3 kg m^{-3}. The thermal enthalpy removed from the atmosphere by rain during any given time step depends on the temperature of the rain during that time step; hence the enthalpy removed from tube i between time 0 and time τ is

$$\left(E_{R_i}\right)_\tau = \sum_{t=0}^{\tau} c_\ell (\delta R_{1,t}) A_i T_{1,K,t} \tag{3-11}$$

where $(\delta R_{i,t})$ is the amount of rain falling during the time step ending at time t. The appropriate rain temperature is assumed to be the air temperature in the lowest level at that time. (Throughout this study, it is assumed that all the constituents of a parcel of cloudy air at a given position and time have the same temperature.)

Since the enthalpy of rain is not a function of k, summation by tubes is a redundant operation

$$\left[E_R\right]_i = E_{R_i} \tag{3-12}$$

Summation by slabs is equivalent to total summation:

$$\langle E_R \rangle = \left| E_R \right| \tag{3-13}$$

ENERGY CHANGE

Although the distribution of energy by type and location at a given time is of interest, the changes in the course of the cloud simulation are of greater interst. Let the operator Δ represent change from time zero up to some given time τ, or

$$\Delta \phi = \phi_\tau - \phi_0 \tag{3-14}$$

This operator can be applied to energy densities, as given in (2-41) through (2-47), the corresponding energy totals, as indicated in (3-5), or energy summations, as indicated in (3-6) through (3-8). Since the operator Δ is independent of the operators $\langle \ \rangle$, $[\ ]$, and $\{\ \}$, the order of application is immaterial.

In some instances, however, straightforward application of (3-14) leads to the computation of small differences of large quantities, with consequent loss of precision. Wherever possible, this problem was

minimized by factoring out those parts of ϕ that are not time-dependent. This was facilitated by the decomposition of the variables of state in accordance with (2-10). For instance, $\overline{T}$ tends to be two orders of magnitude larger than T', so it is more accurate to compute $\Delta T'$ than ΔT, even though they are ostensibly identical.

The reference values of u, w, and q_ℓ are all zero, and their perturbed values are small. In earlier versions of the model, q_v was treated as though its reference value were zero even though q_v varies in a narrow range about a value some two orders of magnitude larger than q_ℓ. In a later version, q_v was decomposed in the same manner as the other variables, but this appeared to have little effect on the energy changes.

In practice, application of (3-14) to (2-41) through (2-47) was carried out as follows:

$$\Delta\eta_{K_{i,k}} = \frac{1}{2}\,\overline{\rho}_{a_k}\,\Delta((q_a + q_v + q_\ell)(u^2 + w^2))_{i,k} \tag{3-15}$$

$$\Delta\eta_{P_{i,k}} = g^{z}{}_k\,\Delta\rho_{i,k} \tag{3-16}$$

$$\Delta\eta_{Ta_{i,k}} = c_p\,\overline{\rho}_{a_k}q_a\,\Delta T'_{i,k} \tag{3-17}$$

$$\Delta\eta_{Tv_{i,k}} = c_{pv}\,\overline{\rho}_{a_k}\left(\overline{T}_k\,\Delta q_{v_{i,k}} + \Delta(T'q_v)_{i,k}\right) \tag{3-18}$$

$$\Delta\eta_{T\ell_{i,k}} = c_\ell\overline{\rho}_{a_k}\left(\overline{T}_k\,\Delta q_{\ell_{i,k}} + \Delta(T'q_\ell)_{i,k}\right) \tag{3-19}$$

$$\Delta\eta_{L_{i,k}} = L\overline{\rho}_{a_k}\,\Delta q_{v_{i,k}} \tag{3-20}$$

After (3-15) through (3-20) have been multiplied by $V_{1,k}$ to derive $\Delta E_{K_{1,k}}$, etc., they can be summed by slabs and tubes.

In the present study, rainfall was always zero at time zero, so

$$\Delta E_{R_1} = E_{R_1} \qquad (3-21)$$

FLUX

If η_θ is the energy density of some particular category θ, then the corresponding vertical flux of energy is

$$F_\theta = w\eta_\theta \qquad (3-24)$$

Any variable property ϕ can be divided into a time-averaged part and a departure:

$$\phi = \tilde{\phi} + \phi'' \qquad (3-25)$$

where, if there have been $n - 1$ time steps between the initial time and the final time τ,

$$\tilde{\phi} = \frac{1}{n} \sum_{t=0}^{\tau} \phi_t \qquad (3-26)$$

It should be noted that the decomposition indicated by (3-25) is not the same as that indicated by (2-10). The straight bar $(\overline{})$ implies a horizontal space average at initial time, whereas the tilde $(\tilde{})$ represents a time average at a given location.

From (3-25) and (3-26) it is readily demonstrated that

$$\left.\begin{aligned}
\tilde{\tilde{\phi}} &= \tilde{\phi} \\[4pt]
\widetilde{\phi''} &= 0 \\[4pt]
\widetilde{\alpha\phi} &= \alpha\tilde{\phi}; \qquad \alpha \text{ independent of } t
\end{aligned}\right\} \qquad (3-27)$$

The flux given by (3-24) for a specified location (i,k) and time t can be decomposed in accordance with (3-25)

$$F_{\theta_{i,k,t}} = \left(\tilde{w} + w''_t\right)_{i,k}\left(\tilde{n}_\theta + n_\theta''_t\right)_{i,k}$$

or

$$F_{\theta_{i,k,t}} = \left(\widetilde{wn}_\theta\right)_{i,k} + \left(\tilde{w}n_\theta''_t\right)_{i,k} + \left(w''_t\tilde{n}_\theta\right)_{i,k} + \left(w''n_\theta''\right)_{i,k,t} \qquad (3-28)$$

If (3-28) is time-averaged in accordance with (3-26), and (3-27) is used, there results

$$\tilde{F}_{\theta_{i,k}} = \left(\widetilde{wn}_\theta\right)_{i,k} + \left(\widetilde{w''n_\theta''}\right)_{i,k} \qquad (3-29)$$

Since n_θ is an energy density, the dimensions of (3-29) are $J\ m^{-2}\ s^{-1}$. The terms on the right-hand side of (3-29) can be identified as the flux of the mean energy of type θ with the mean vertical wind (or, more simply, the mean vertical flux) and the eddy vertical flux. The latter expresses the correlation between the vertical wind and energy of type θ.

If each term of (3-29) is multiplied by A_i, the product is the vertical flux through the entire horizontal surface represented by the grid point (i,k). Horizontal summation then gives the total flux through the level designated by k:

$$\langle A\tilde{F}_\theta\rangle_k = \langle \tilde{w}\ A\tilde{n}_\theta\rangle_k + \langle\widetilde{w''\ An_\theta''}\rangle_k \qquad (3-30)$$

It is convenient to define two types of horizontal mean. The ordinary one for any function $\phi_{i,k}$ of i and k is

$$\overline{\phi_k}^S = \frac{1}{I}\ \langle\phi\rangle_k \qquad (3-31)$$

since the number of terms in the slab summation is I. The area-weighted horizontal mean is

$$\overline{\phi}_k^A = \frac{\langle A\phi \rangle_k}{\langle A \rangle} \qquad (3\text{-}32)$$

It follows that

$$\overline{\phi}_k^A = \frac{I\overline{A\phi}_k^S}{\langle A \rangle} \qquad (3\text{-}33)$$

(Note that $\overline{\phi}_k^S$ and $\overline{\phi}_k^A$ may also be functions of time, but $\overline{\phi}_k$ represents the reference state at initial time.) By analogy to (3-25), any function of i can be broken into a slab-averaged part and a departure:

$$\phi_{i,k} = \overline{\phi}_k^S + \phi^*_{i,k} \qquad (3\text{-}34)$$

If we make the definition

$$\xi_\theta = A\eta_\theta \qquad (3\text{-}35)$$

and note that A is independent of t, (3-30) becomes, through the use of (3-31),

$$I\,\overline{(A\widetilde{F}_\theta)}_k^S = I\,\overline{(\widetilde{w\xi}_\theta)}_k^S + I\,\overline{(\widetilde{w''\xi_\theta''})}_k^S \qquad (3\text{-}36)$$

By means of (3-34)

$$(\widetilde{w\xi}_\theta)_{i,k} = \overline{\widetilde{w}}_k^S\,\overline{\widetilde{\xi}_\theta}_k^S + \overline{\widetilde{w}}_k^S\,\widetilde{\xi}_{\theta\,i,k}^* + \widetilde{w}_{i,k}^*\,\overline{\widetilde{\xi}_\theta}_k^S + \widetilde{w}_{i,k}^*\,\widetilde{\xi}_{\theta\,i,k}^* \qquad (3\text{-}37)$$

With the use of identities analogous to those of (3-27), the slab average of (3-37) becomes

$$\overline{(\widetilde{w\xi}_\theta)}^S_k = \overline{\widetilde{w}}^S_k \ \overline{\widetilde{\xi}_\theta}^S_k + \overline{(\widetilde{w}^{\star}\widetilde{\xi}_\theta^{\ \star})}^S_k \tag{3-38}$$

Substitution of (3-38) into (3-36), followed by use of (3-35), yields

$$\overline{I(A\widetilde{F}_\theta)}^S_k = \overline{\widetilde{w}}^S_k \ \overline{I \ A\widetilde{n}_\theta}^S_k + \overline{I \ A(\widetilde{w}^{\star} \ \widetilde{n}_\theta^{\ \star})}^S_k + \overline{I \ A(\overbrace{w'' \ n_\theta''})}^S_k \tag{3-39}$$

If (3-39) is divided by $\langle A \rangle$ and (3-32) is used, there results

$$\overline{\widetilde{F}_\theta}^A_k = \overline{\widetilde{w}}^S_k \ \overline{\widetilde{n}_\theta}^A_k + \overline{(\widetilde{w}^{\star} \ \widetilde{n}_\theta^{\ \star})}^A_k + \overline{(\overbrace{w'' \ n_\theta''})}^A_k \tag{3-40}$$

In (3-40) $\overline{\widetilde{F}_\theta}^A_k$ represents the vertical flux of energy of type θ through the horizontal surface designated by k, averaged both horizontally and in time. The dimension is $J \ m^{-2} \ s^{-1}$, and it yields a single value for each level k. The first term on the right-hand side is the flux of the doubly averaged energy by the doubly averaged vertical wind; it can be called the mean flux over the slab as distinguished from the corresponding term of (3-29), which is the mean flux at a grid point. The other two terms of (3-40) represent two types of eddy flux. The first of these two is associated with standing waves (or circulations approximating them). Inspection of Figs. 13 and 14 reveals that such circulations do exist in this model. The remaining term represents transient eddies.

The summation $\sum\limits_{k=1}^{K} \overline{\widetilde{F}_\theta}^A_k$ can be thought of as representing the rise or fall of the "center of energy" (analogous to the center of mass) of energy of type θ. Some computations of this quantity are shown in Fig. 20.

The entire foregoing development for energy flux is also appli-
cable to mass flux. For example, to study the flux of water vapor, it
is merely necessary to replace η_θ in the above equations with $\bar{\rho}_a q_v$.

The accumulation or depletion of energy in a given layer is found
by vertical differencing of (3-30). This is a measure of the divergence
of energy, and it may be represented by

$$\mathcal{B}_{k+\frac{1}{2}}(\breve{F}_\theta) = \langle A\widetilde{F}_\theta \rangle_k - \langle A\widetilde{F}_\theta \rangle_{k+1} \tag{3-41}$$

Since the indexing system is oriented so that k increases as z
decreases, (3-41) will have a negative value in the case of convergence
and a positive value in the case of divergence. That is, if (3-41) is
negative, it indicates an increase in energy of type θ in the layer
between k and k + 1. Of course, none of the flux calculations tell
anything about any transformations of energy that might be occurring.

IV. ENERGY DISTRIBUTION AND TRANSFORMATION

Materials used in the present analysis comes from two cloud-simulating computations reflecting different stages in development of the study. Table 1 summarizes the initial conditions, some properties of the clouds produced, and certain aspects of the computation. Cloud B is computed from the San Juan sounding of 20 August 1963 (see Fig. 1) and is similar to Cloud 3 of Murray and Koenig (1972). Cloud A differs

Table 1

SOME CLOUD PROPERTIES

Property	Cloud A	Cloud B
Atmospheric sounding	Smoothed, San Juan, 2300 GMT, 20 Aug. 1963	Unsmoothed, San Juan, 2300 GMT, 20 Aug. 1963
Perturbation	Momentum	Humidity (net change equal to zero)
Base	1.2 km	1.2 km
Height		
Maximum	5.8 km	6.0 km
Time of maximum	25 min	35 min
Radius		
Maximum	0.6 km	0.6 km
Time of maximum	20 min	30 min
Temperature departure		
Maximum	2.1°C	2.3°C
Time of maximum	15 min	25 min
Vertical draft		
Maximum	18 m sec^{-1}	15 m sec^{-1}
Time of maximum	20 min	30 min
Height of maximum	4.2 km	4.8 km
Life time	50 min	55 min
Total condensate	3558 tons	
Rain amount	282 tons	4693 tons
Conservation applied?	Yes	No
Eddy diffusion?	Yes	Yes

NOTE: Time step ≤ 12 sec
       Time resolution = 5 min
       Distance resolution = 0.2 km

from Cloud B in three main characteristics: (a) the sounding was slightly smoothed with respect to temperature and strongly smoothed with respect to dewpoint (see Fig. 2); (b) the initial perturbation was of momentum rather than humidity; and (c) a computational scheme was included to assure the conservation of mass of water substance. Because of this third characteristic, Cloud A is considered to be the more useful of the two. Cloud B is used mainly to study the vertical flux of various categories of energy, a feature that is not highly sensitive to either conservation of mass of water substance or non-smoothed soundings but that is sensitive to a perturbation of the vertical wind.
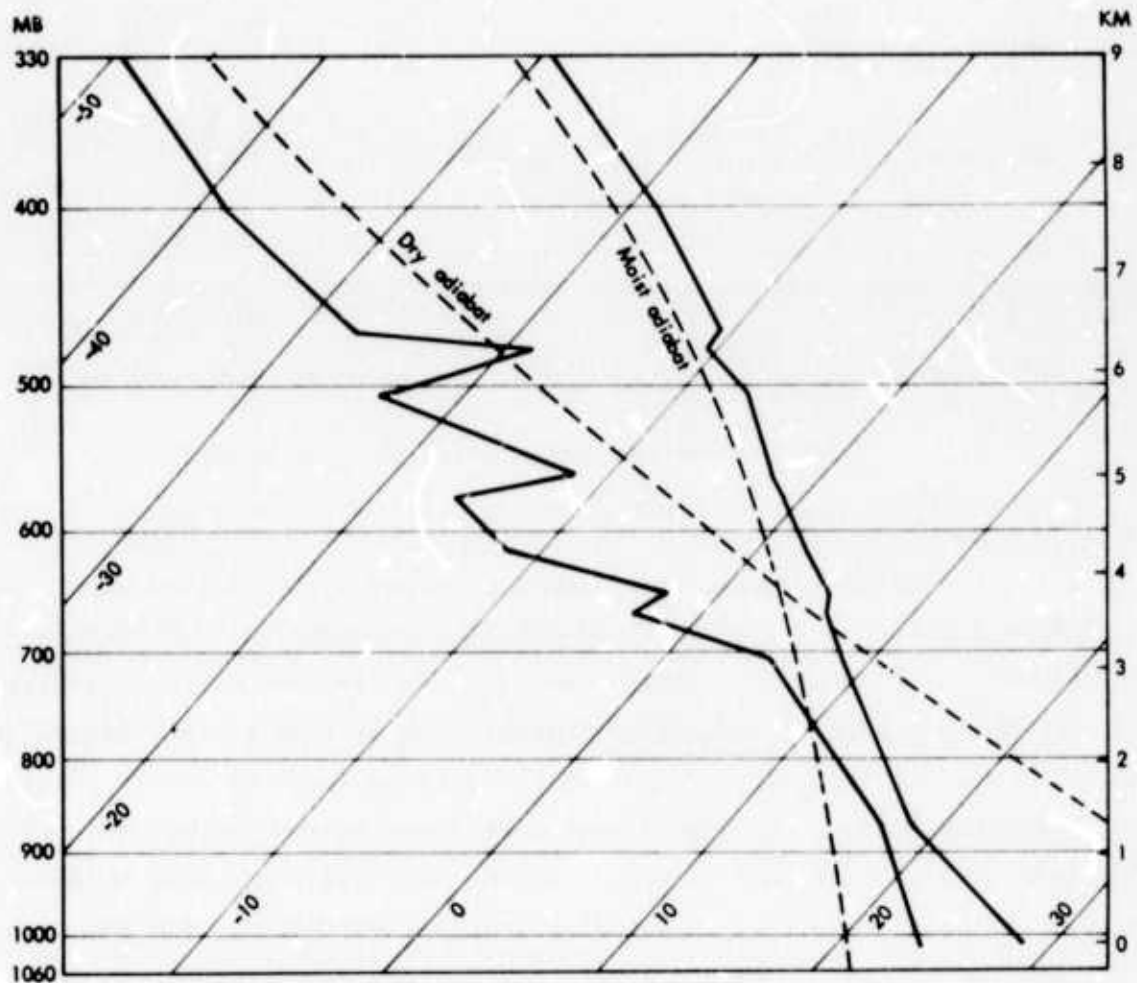

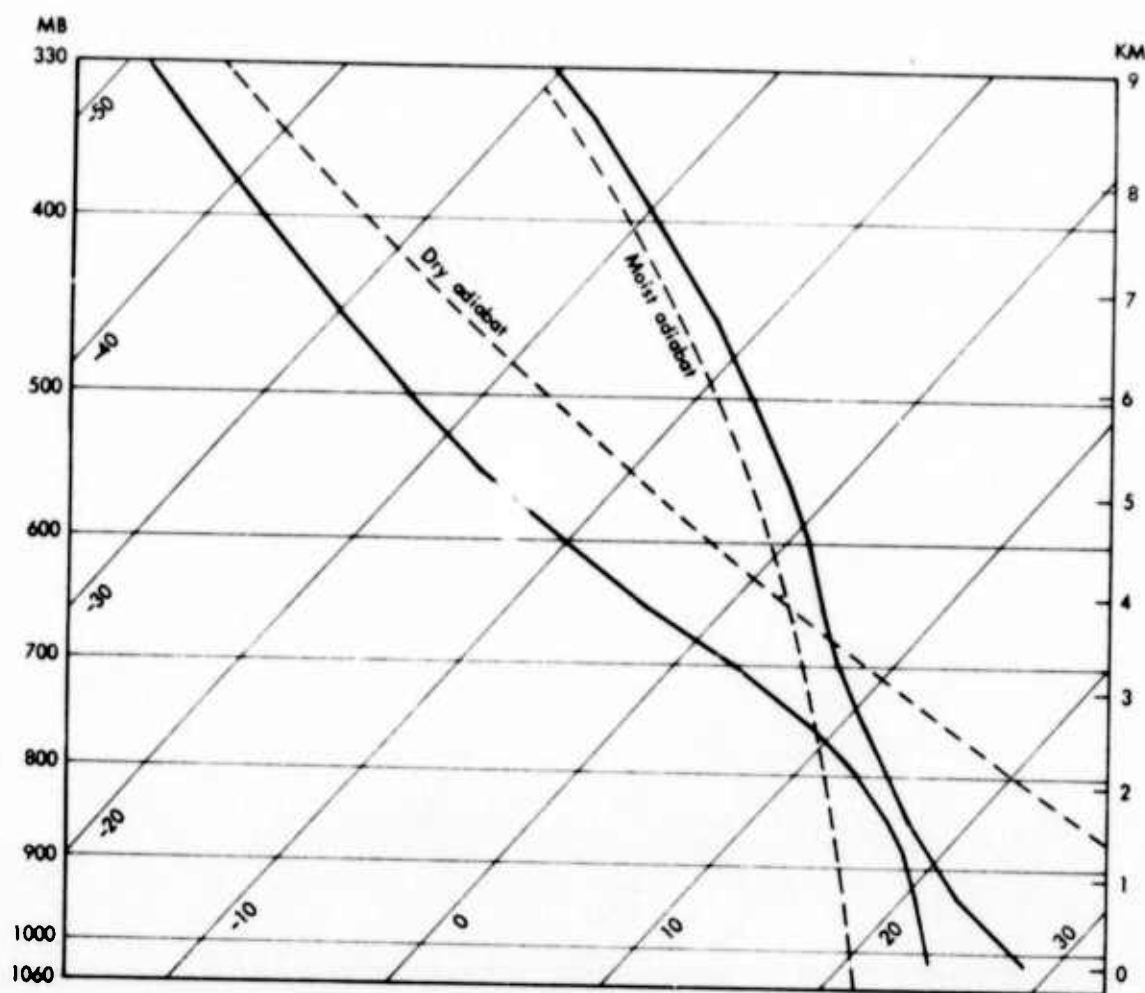Fig. 1—Sounding for San Juan, 2300 GMT, 20 August 1963, used for Cloud B

Fig. 2—Smoothed version of San Juan sounding, used for Cloud A

The initial impulse of Cloud A provided a circulation with a max-imum updraft of 3.5 m sec^{-1}, thereby introducing 7.5×10^9 joules (0.0075 terajoules) of kinetic energy into the computational domain. If no condensation occurs, an impulse such as this rapidly decays and there is little rearrangement of the various forms of energy. The humidity impulse of Cloud B introduced more energy in the form of enthalpy into the active cloud region, but this was counterbalanced by an equal reduction in enthalpy in the environment. The momentum impulse of Cloud A caused a more rapid cloud development than did the humidity impulse of Cloud B.

The evolution of Cloud A is summarized in Table 2. The top of the table depicts, at five-minute intervals, the total mass of condensed

Table 2

CHARACTERISTICS OF CLOUD A

Category	Mass of Water of Various Categories in Metric Tons at Given Times (min)												
	0	5	10	15	20	25	30	35	40	45	50	55	60
Cloud water mass	0	432	570	935	1152	699	363	116	27	5	0.6	0	0
Rain mass	0	0	1	25	84	172	258	280	287	282	282	282	282
Condensed water[a]	0	518	1054	1934	3155	3535	3558	3558	3558	3558	3558	3558	3558

Type of Energy	Change in Energy in TJ from Initial Time to Given Time (min)				Base Energy[b] at t = 0 in Domain (TJ)
	15	30	45	60	
Thermal enthalpy of liquid	+1.11	+0.436	+0.006	0	0
Thermal enthalpy of water vapor	-0.425	-0.230	-0.128	-0.138	3177.
Thermal enthalpy of dry air	+3.77	+5.14	+4.15	+3.93	221180.
Latent enthalpy	-2.34	-1.34	-0.719	-0.706	14847.
Thermal enthalpy of water vapor plus air	+3.34	+4.91	+4.03	+3.79	236027.
Kinetic energy	+0.001	-0.0061	-0.0066	-0.0068	0.0075
Potential energy	-2.66	-6.44	-5.94	-5.73	29756.
Total[c]	-0.67	-2.44	-2.64	-2.66	2.7×10^5
Rain thermal enthalpy	+0.001	+0.22	+0.35	+0.35	

[a] Amount actually condensed, not the amount present. The latter is given by the sum of cloud and rain mass. Evaporation concurrent with condensation causes the mass of condensate to be less than the mass condensed.

[b] Energy of a given kind is computed from expressions shown in Secs. II and III. Since the value has not been found by integration from a base level, the values shown are not true total energy values, but merely furnish an idea of the magnitude of the energy being considered. Energy sums are expressed in terajoules: 1 TJ = 10l2 J.

[c] Total energy is the sum of latent enthalpy, thermal enthalpy, potential energy, and kinetic energy. The pressure work term is not considered in this study.
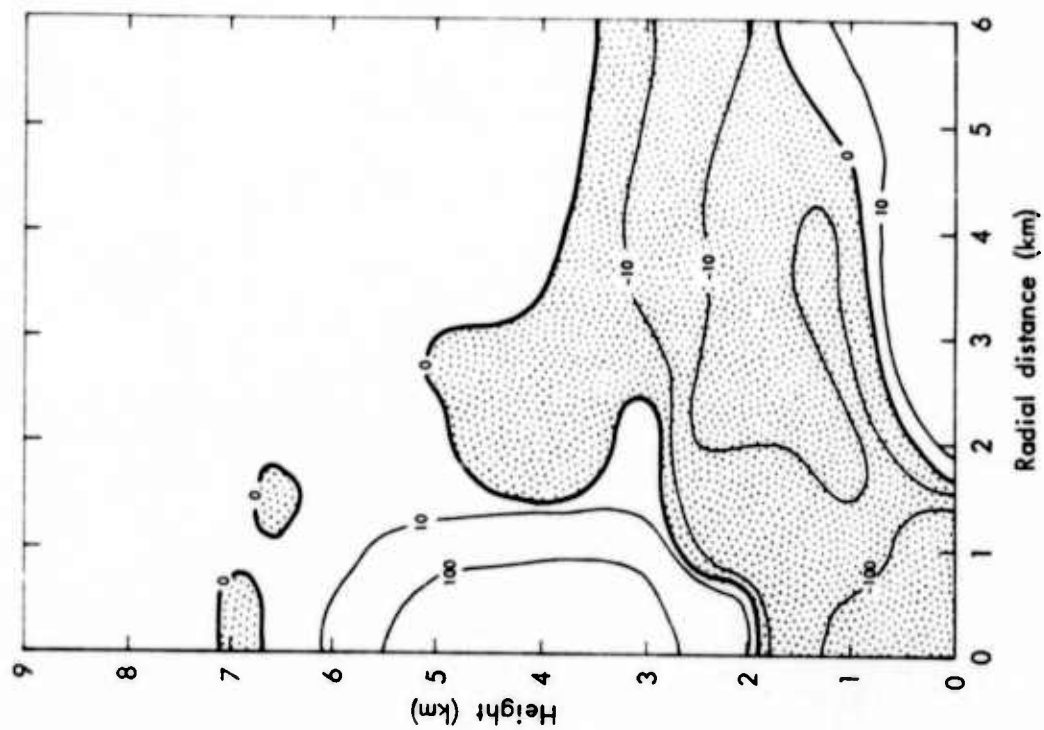
water in the domain, both airborne (cloud water mass) and on the ground
(rain mass), and also the cumulative mass of water that has been con-
densed up to the given time. This is always larger than the sum of the
other two categories because some of the condensate later evaporates.
The lower part of Table 2 shows the change in energy content of various
types from initial time up to 15, 30, 45, and 60 minutes. The right-
hand column gives the base level from which the changes occur. Except
for the thermal enthalpy of liquid and the kinetic energy, the base
levels are all much larger than the changes. The degree to which energy
is conserved is shown by the totals to be 1 part in 10^5.

Essentially no new condensation occurred after 30 minutes; i.e.,
the cloud was virtually dead from that time on. The latent enthalpy,
thermal enthalpy, and potential energy changes also indicate that the
cloud is in decline after 30 minutes. The kinetic energy is nearly
constant during the later period, but it is less than the initial per-
turbation, and examination of the fields of motion shows that the
circulations are much less organized. Rainout and evaporation erode
the cloud until it finally disappears after 55 minutes.

The rearrangements of energy of Cloud A are shown in Figs. 3 through
7 in the form of fields of change of energy density, expressed in joules
per cubic meter per hour. As shown in Table 1, the volume actually
occupied by the cloud extends from 1.2 km up to 6 km and from the axis
out to 0.6 km. These limits approximate the envelope of the cloud
boundary over the lifetime of the cloud. Figure 8 shows the change of
energy content of each type after being summed over horizontal slabs
in accordance with (3-6), and Fig. 9 shows the corresponding changes
after summation over vertical tubes in accordance with (3-7). When
summed by slabs or tubes, energy is expressed in terajoules (10^{12} joules)
and energy change in terajoules per hour. All changes shown in these
figures are taken from time zero (before the inception of convection
but after the implementation of the perturbation) to 60 minutes (after
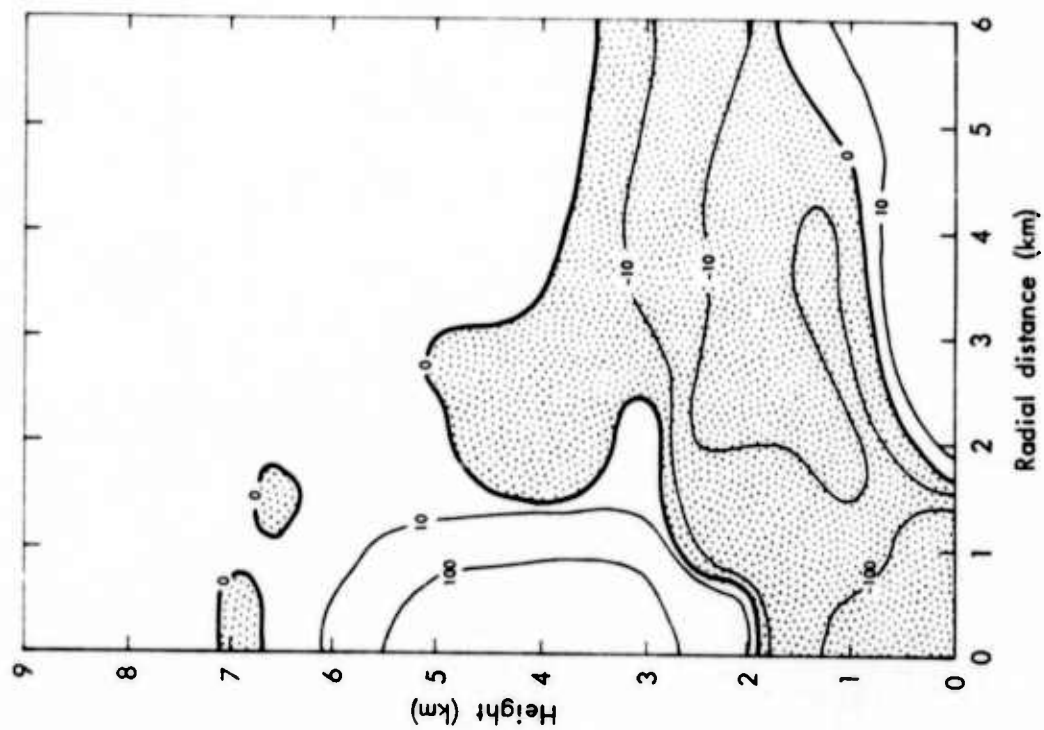completion of the life cycle of the cell).

LATENT ENTHALPY

Changes in the latent enthalpy are shown in Figs. 3, 8(a), and 9(a)
for Cloud A. Increases in latent enthalpy occur in regions that become

NOTE: Regions of decrease are shaded.

Fig. 4—Change from 0 to 60 min of thermal enthalpy density of water vapor (J m^{-3} hr^{-1}), Cloud A

NOTE: Regions of decrease are shaded.

Fig. 3.—Change from 0 to 60 min of latent enthalpy density (J m^{-3} hr^{-1}), Cloud A

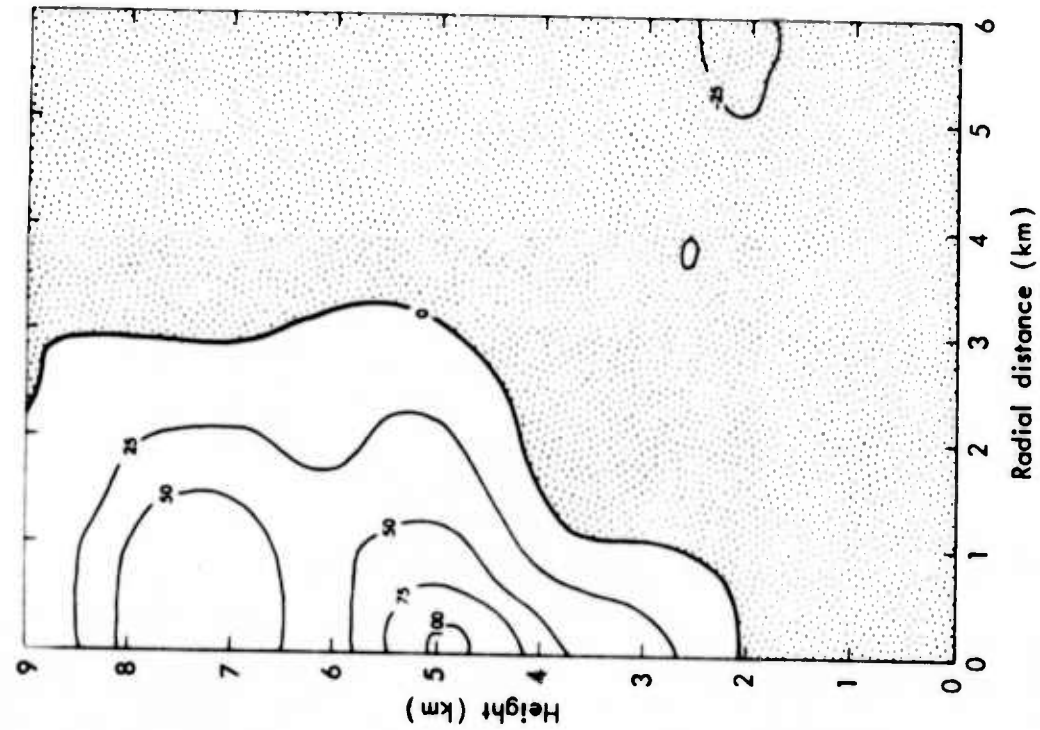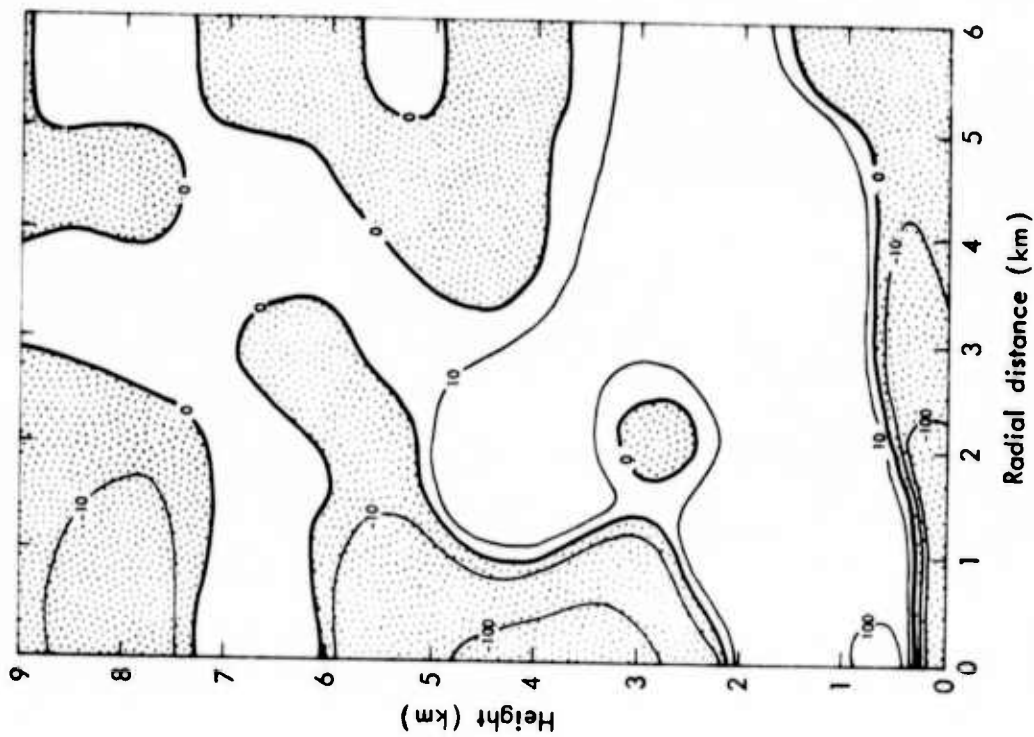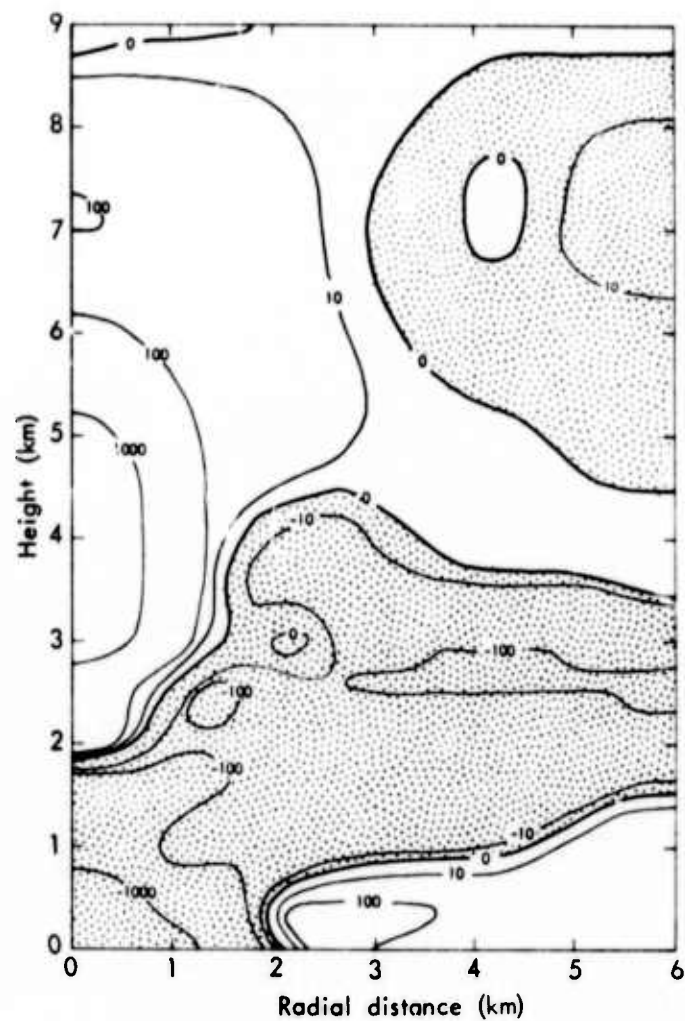NOTE: Regions of decrease are shaded.

Fig. 6—Change from 0 to 60 min of potential energy density
(J m⁻³ hr⁻¹), Cloud A

NOTE: Regions of decrease are shaded.

Fig. 5—Change from 0 to 60 min of enthalpy density
of dry air (J m⁻³ hr⁻¹), Cloud A

NOTE: Regions of decrease are shaded.

Fig. 7—Change from 0 to 60 min of static energy density
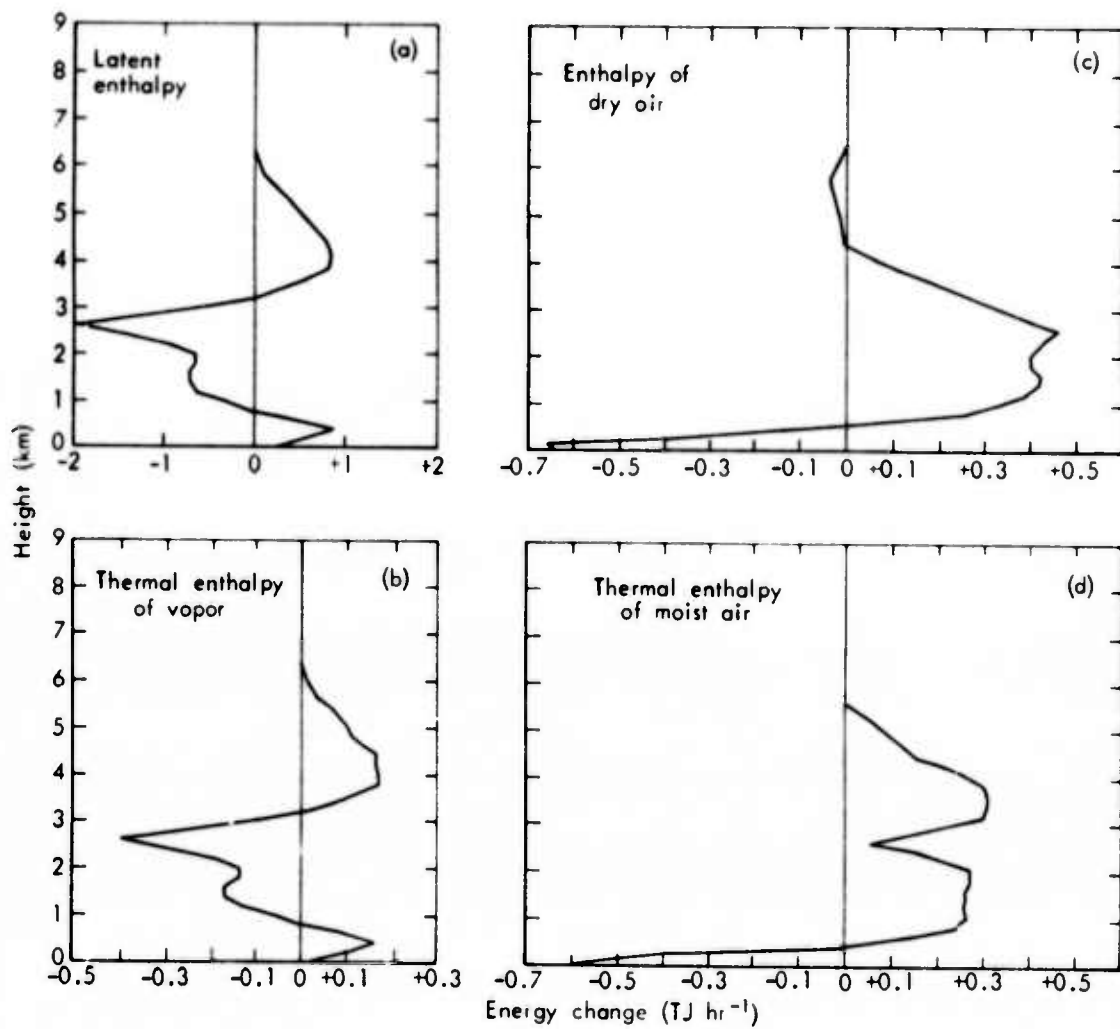$(J\ m^{-3}\ hr^{-1})$, Cloud A

Fig. 8—Change from 0 to 60 min of energy summed by slabs (TJ hr^{-1}), Cloud A
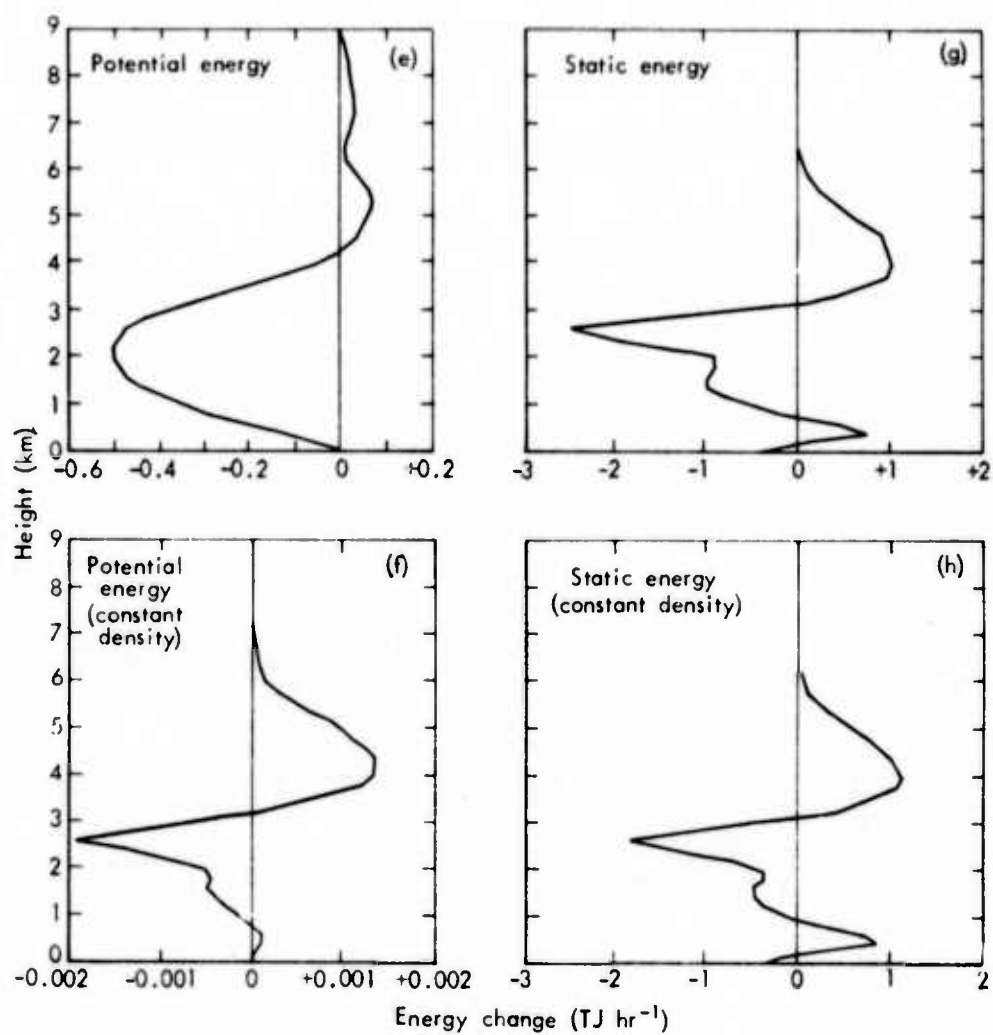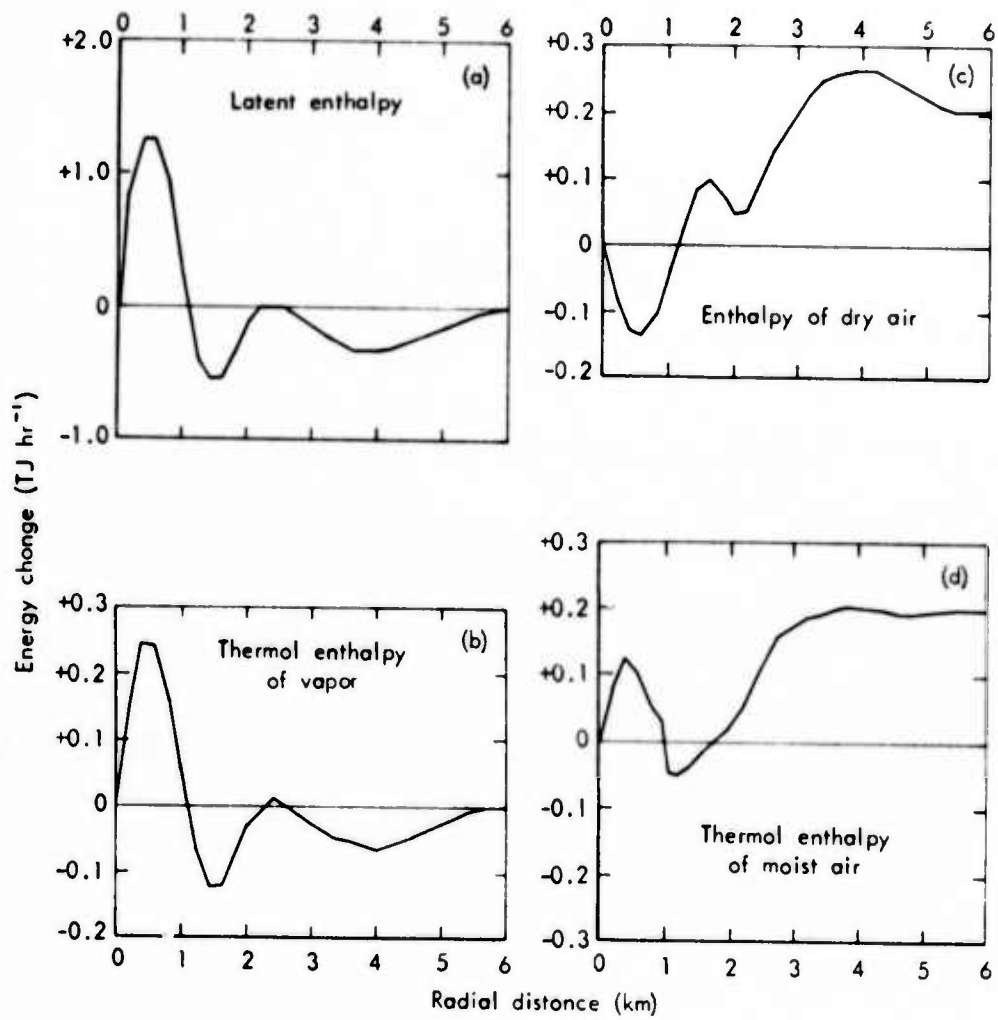
Fig. 8 — (e - h)

Fig. 9—Change from 0 to 60 min of energy summed by tubes (TJ hr⁻¹), Cloud A
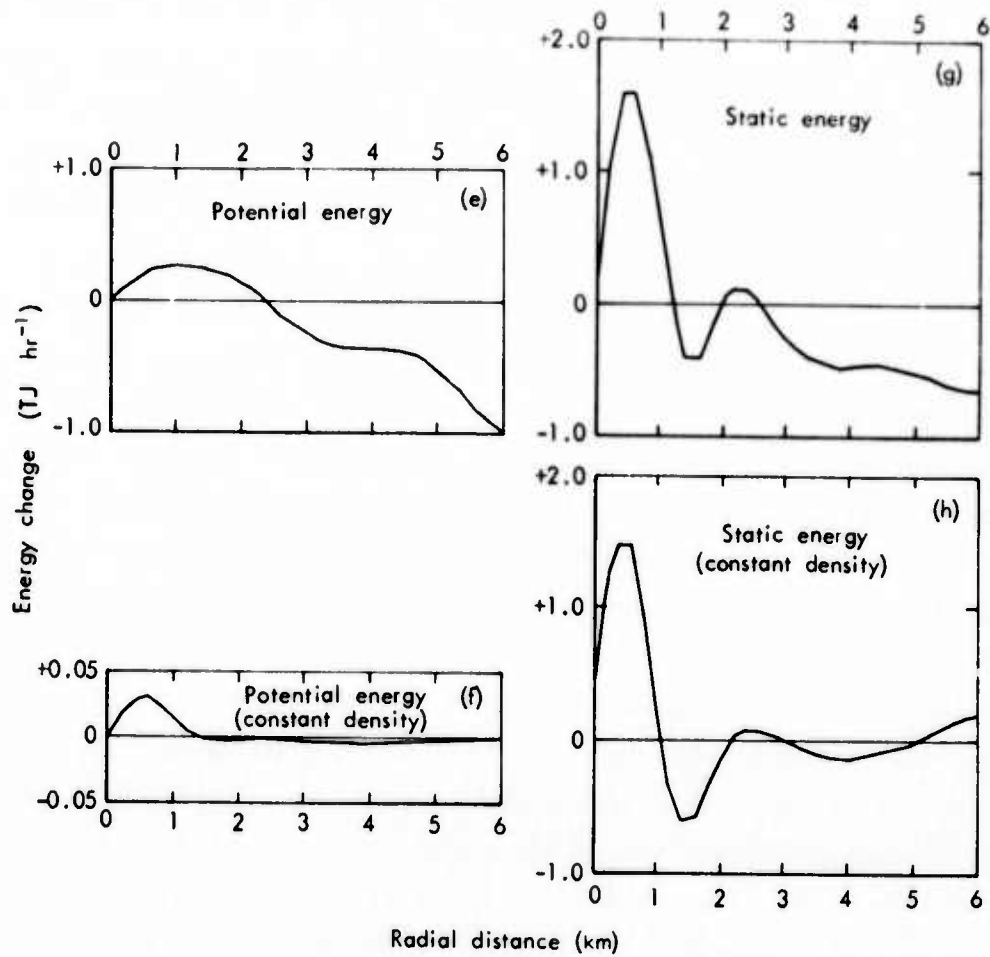
Fig. 9 — (e - h)

richer in water vapor at the expense of those that become poorer, for latent enthalpy is directly related to the mass of water vapor. As revealed in Fig. 3, the entire region beneath the cloud, and a large volume encircling the cloud and extending vertically from the cloud base to about half the height of the cloud, has decreasing latent enthalpy, the result of downward advection of drier air in the region distant from the cloud and of upward advection of moister air into the cloud itself. The dying cloud leaves behind a pocket of increased latent enthalpy that is larger in volume than the cloud itself. Near the cloud, the changes in latent enthalpy are relatively large in magnitude (maximum values near 4000 J m^{-3}), and the gradients are intense.

The overall vertical movement of latent enthalpy is shown in Fig. 8(a). There are increases in latent enthalpy at levels below that of the cloud base (~ 1.2 km) and throughout the volume in which the upper half of the cloud resides. These are offset by decreases through the volume in which the lower half of the cloud resides. (The slabs over which enthalpy is summed cover the entire horizontal extent of the domain, not just the part occupied by the cloud.) The subcloud increase is in the region several cloud radii away from the cloud itself and apparently is caused by convergence of the horizontal outflow associated with the moist downdraft. The middle level decrease occurs in the region on which the cloud feeds, and the upper level increase is caused by the evaporation of water in the dying cloud. The net change is negative because of the removal of rainwater formed by condensing water vapor.

The overall horizontal movement of latent enthalpy is shown in Fig. 9(a). These data show a marked increase in latent enthalpy in the cylinder occupied by the cloud coupled with decreases in the air away from the cloud. (The downturn in all the curves of Fig. 9 as the central axis is approached is a result of the dependence on the square of radial distance; see Eq. (3-1).) About 2 cloud radii from the central axis (i.e., about 1.5 km) there is a minimum point on the curve, and there is a relative maximum at 3 cloud radii (2.3 km). Reference to Fig. 3 clearly shows the minimum to be related to the depletion rear the cloud base and the cloud edge. The small maximum is evidently due mainly to the convergence of vapor evaporated in the downdraft and the rain shaft and carried away from the axis by the shallow outdraft near the ground surface. This outdraft is shown in Fig. 13, which is indicative of the circulations in Cloud A even though the data are actually from Cloud B. There is also a contribution from a little "ledge" that separates the subcloud and lateral vapor depletion regions. This small anomaly is located at the top of the moist layer of the undisturbed atmosphere and in a shearing zone between the mean circulation cells below and to the side of the cloud.

Brown (1967), following the suggestion of Braham (1952) defined the available energy of a cloud as the latent heat that has been released by condensation. Using a number of measurements of "cloud mass"

(i.e., measured cloud volume times the density of the ambient air) and assumed liquid water content for different types of clouds, he developed an empirical formula for available energy as a function of cloud mass. Brown's available energy is comparable to the change of latent enthalpy computed in the present study. However, application of Brown's formula to Cloud A yields a value of 14.5 TJ as compared with our computed value of 1.34 to 2.34 TJ (see Table 2). Two reasons for the disparity may be mentioned. Our measure of "cloud mass" assumed that the cloud was a cylinder of 600 m radius and 4.6 km depth, which is the approximate envelope of the cloud, but at no particular time during the computation did the cloud entirely fill the cylinder. The more important reason is that Brown assumed a uniform and rather large value of liquid water content throughout the cloud, whereas our computations yielded much smaller values throughout the major part of the cloud. In view of these differences and of the fact that Brown claimed only order-of-magnitude accuracy for his formula, the two studies working from entirely different premises give comparable results.

THERMAL ENTHALPY

The total change in thermal enthalpy can be divided into two terms, one representing water vapor (e.g., (3-18)), the other dry air (e.g., (3-17)). Since no liquid was present at $t = 0$ or $t = 60$, the net change in thermal enthalpy of liquid was zero. The change in the density of thermal enthalpy of water vapor is shown in Fig. 4. The pattern largely reflects the change in water vapor content rather than temperature changes, and therefore is similar to the pattern displayed by the change in latent enthalpy. The size of the change, however, is about one order of magnitude smaller. The patterns of vertical and horizontal movement of thermal enthalpy of water vapor are shown in Figs. 8(b) and 9(b). Again, the rearrangement of this form of energy is similar to that of latent enthalpy.

The change in the density of thermal enthalpy of dry air is shown in Fig. 5. When $\bar{\rho}_a$ is used in energy density computations, as it is in all categories but potential energy, the mass of dry air remains constant at each grid point, and therefore the changes in enthalpy of dry

air are directly related to changes in temperature. It is noteworthy that near the cloud the pattern of change in enthalpy of dry air is somewhat similar to that of thermal enthalpy of water vapor except that the sign is reversed. The cloud evaporates leaving behind wetter but cooler air. The magnitude of the change is similar (i.e., small compared with latent enthalpy changes).

The region occupied by the cloud loses energy in the form of enthalpy of dry air (except near the level of the cloud base) and the subcloud region (except close to the ground) gains energy in that form. The loss of energy in the upper part of the cloud directly reflects the cooling by evaporation of the condensate that does not fall out as rain. The loss of energy near the ground is caused by the evaporative cooling of rain in the downdraft near the ground and the outward spread of this cooled air. A large volume of air receives modest increases in enthalpy. This is caused by the (generally) slowly sinking air that compensates for the upward motions within the cloud itself. The region of warming includes the subcloud layer, except near the ground, and extends upward outside the cloud to a level about four-fifths of the cloud height above the cloud base. The horizontal extent of the warming is at least 5 cloud radii. At distances greater than 7 cloud radii ($\sim$ 4200 m) the pattern becomes less distinct.

The vertical rearrangement of enthalpy of dry air is depicted in Fig. 8(c), which clearly shows the loss of energy in the outflow caused by the cool downdraft, the gain in energy in the air between the downdraft outflow and the upper mid-region of the cloud, and the loss of energy in the vicinity of the upper region of the cloud.

The horizontal rearrangement of enthalpy of dry air is shown in Fig. 9(c). Columns of air from the axis to a point somewhat beyond the cloud radius lose energy, and an increase beyond that point is clearly shown. The fact that the change does not approach zero at the outer boundary of the computational domain is considered an unrealistic feature related to the closed nature of the domain. The closed boundaries presumably lead to general subsidence that is greater than that found in nature. That is, near the boundary of the domain the air moves downward a greater distance than would occur in nature and the

effect of the cloud is stronger at a greater distance than would be evident in nature.

THERMAL ENTHALPY OF MOIST AIR

It was noted previously that changes in the thermal enthalpies of dry air and water vapor are similar but of opposite sign. The water vapor contribution to change in thermal enthalpy of moist air will dominate in regions close to the cloud.

The vertical rearrangement of thermal enthalpy of moist air is shown in Fig. 8(d). The effect of evaporation in the downdraft below the cloud and the warming outside the cloud at the level of the cloud base are clear even after horizontal summation. The increase in thermal enthalpy in the slabs at the height of the upper portions of the cloud is caused by the additional water content injected by the evaporation of cloud debris at that level.

The horizontal rearrangement of thermal enthalpy of moist air is shown in Fig. 9(d). The contrasting dominance of the transport of water vapor content in the vicinity of the cloud, of evaporative cooling at the edge of the cloud, and of the heating caused by compensating sinking motions away from the cloud are clearly shown.

POTENTIAL ENEF

As shown in Fig. 6, potential energy increases in the upper portion of the cloud and out to about 5 cloud radii, and decreases below the cloud. There are decreases in potential energy over most of the domain external to the cloud except directly above it. The absolute value of the change in energy density is not a marked function of radius, except close to the cloud itself. At high altitude, even near the outer boundary of the domain, absolute values of potential energy change are of the order of 10 J m^{-3}. This is a relatively large value at distances remote from the cloud, the latent enthalpy and thermal enthalpy changes being about one order of magnitude smaller.

Potential energy density is the only category computed with the use of an air density that was allowed to vary as temperature and pressure vary from their basic states. If $\bar{\rho}_a$ rather than ρ_a were used in

computing potential energy density, as it is for other energy densities, there would be little variation beyond about 1.5 km radial distance, as is shown by Fig. 9(f). However, when the air density varies, the potential energy varies throughout the domain. In particular, Fig. 9(e) shows decreasing potential energy with increasing radius, illustrating the influence of nearly constant subsidence combined with the effect of the square of radial distance. Figure 8(e), using ρ_a, and Fig. 8(f), using $\bar{\rho}_a$, also show striking differences in the vertical. In general, with variable density, as is required for consistency, the pattern is smoother. The overall change in potential energy is negative, the lower portion of the atmosphere losing more energy than the upper portion gains.

Some further questions regarding the calculation of potential energy are discussed in Sec. VI.

STATIC ENERGY

The overall change in the stability of the atmosphere is indicated by changes in the static energy, which is the sum of thermal enthalpy, latent enthalpy, and potential energy. These changes are shown in Fig. 7, and, not surprisingly, they largely reflect changes in latent enthalpy. The lower atmosphere close to the cloud loses energy, while in the vicinity of the upper and middle portions of the cloud the atmosphere gains energy. This situation extends horizontally for a distance of several cloud radii (and, because of diffusion and mixing with the environment, would extend even farther if the computation continued past the lifetime of the cloud). This rearrangement of energy tends to stabilize the atmosphere. At greater distances the situation is reversed. The lower atmosphere receives energy while the upper atmosphere loses it. This causes destabilization of the atmosphere and increases the likelihood of convective activity. The magnitude of the change toward destabilization, however, is much smaller than that for stabilization near the cloud. Inspection of Fig. 7 and similar figures for changes over shorter time intervals suggests that the greatest destabilization occurs at a distance of about 5 cloud radii from the axis and at the end of the life cycle of the parent cloud. This would

be approximately the region of convergence related to the outward
spreading downdraft, and, consequently, one might suppose that this
would be a favorable location for new convective activity. The dis-
tance is, of course, time-dependent both from the standpoint of changes
in vertical energy content and downdraft/outflow convergence.

Vertical changes in static energy throughout the domain (slab-
summed) are shown in Fig. 8(g). The dominance of the water vapor
transport is again revealed in this figure, and the overall stabili-
zation of the atmosphere is apparent.

Horizontal changes (tube-summed) in static energy are shown in
Fig. 9(g). Again, the dominance of water vapor transport and the
latent enthalpy term are apparent. The cloud is clearly shown to be
a region in which energy is concentrated and lifted at the expense of
a large surrounding volume. From Fig. 9(g) one might suspect that the
effective influence of the cloud extends about 5 cloud radii--a value
similar to that suggested for preferred additional convective activity.
Again, this effective volume is time-dependent and the present remarks
refer to the situation at the end of convection.

ENVIRONMENT STABILIZATION

A key function of cumulus convection is to relieve potential in-
stability in the vertical structure of the atmosphere. It does so by
transferring static energy upward.

The static energy density profile (in kilojoules per cubic meter)
of the environment for Cloud A is shown in Fig. 10, together with the
change that occurred along the cloud axis as a result of convective
activity. The corresponding changes summed over entire slabs are
shown in Fig. 8(g). The movement of static energy upward is apparent
in both figures. However, if the specific static energy (energy per
unit mass of moist air) is viewed, as in Figs. 11 and 12, a clearer
picture emerges.

In Fig. 11 a minimum in specific static energy is evident at a
height of 5 km. Since static energy is a very nearly conservative
property, any mass of air rising from a level lower than 5 km should
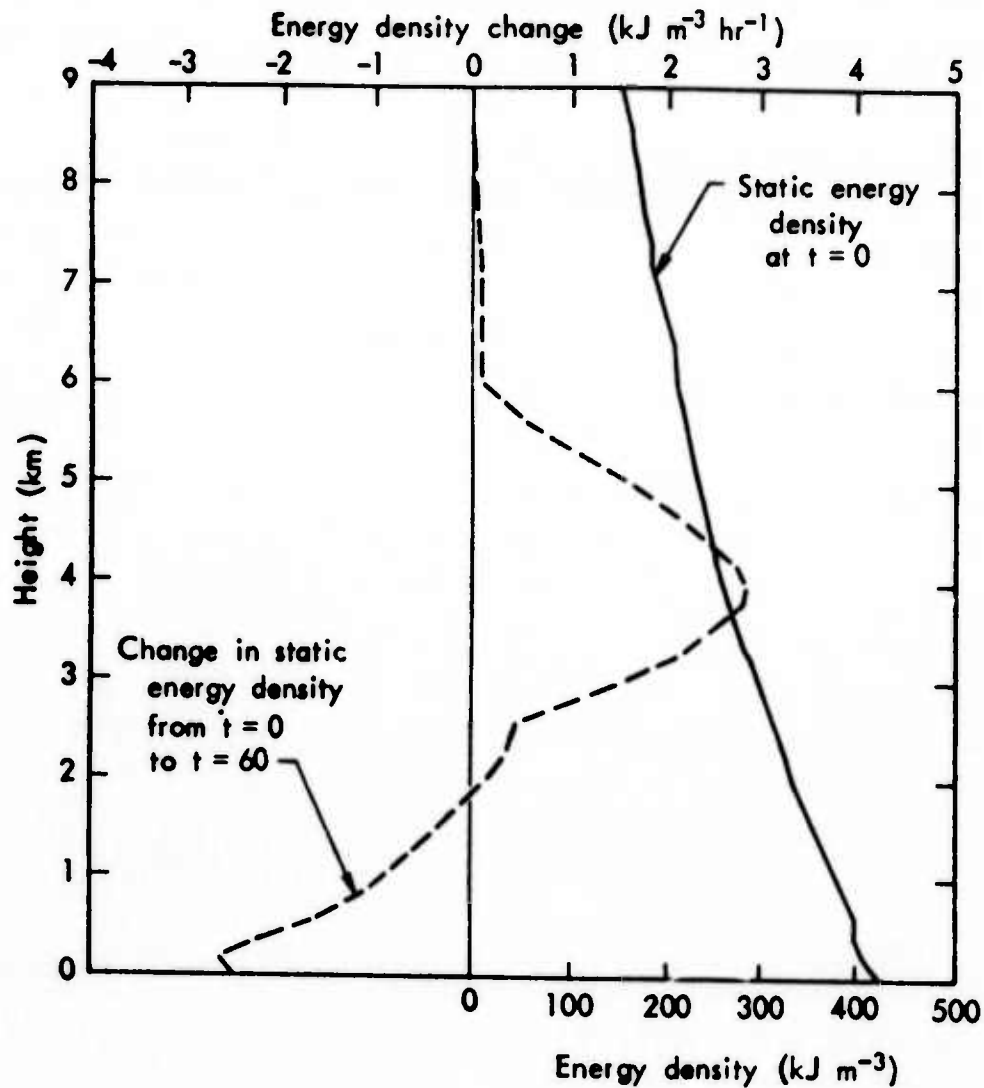remain buoyant until it reaches at least 5 km regardless of mixing

Fig. 10—Static energy density (lower scale) and its change from 0 to 60 min
(upper scale) on the central axis of Cloud A

with external air (entrainment). If no entrainment occurs, the parcel
should rise until it reaches a height somewhere above 5 km, at which
the specific static energy equals that of the parcel. If entrainment
occurs, the static energy of the rising parcel will continuously de-
crease and the parcel will not rise so high. Strong entrainment may
cause the static energy of the parcel to approach that of the environ-
ment and the cloud will not rise much above the level of minimum static
energy (5 km in this case). If the cloud is poorly organized and mix-
ing and diffusion are intense, the parcel will have a specific static
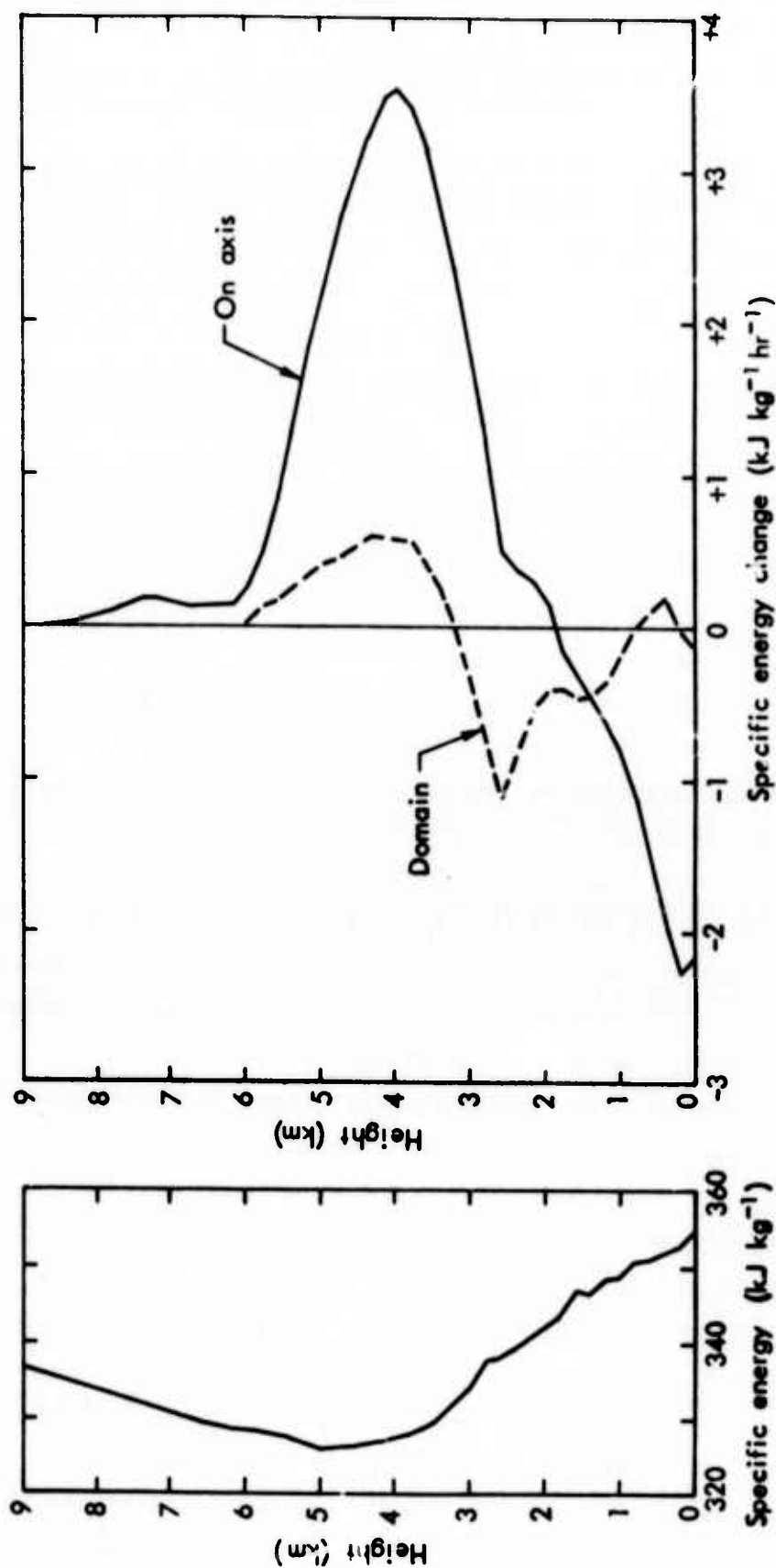energy very close to that of the environment, and drag forces will

Fig. 12—Change in static energy per unit mass of moist air from 0 to 60 min on the central axis of Cloud A, and horizontally averaged over the entire domain

Fig. 11—Static energy per unit mass of moist air at time 0, Cloud A

prevent it from rising. Thus, the height of rise of the cloud tower is dependent on the degree of entrainment.

Mixing, or entrainment, is a surface effect, whereas the total energy in a cloud is volume-dependent. Thus, the larger the cloud radius, the less will be the mixing in proportion to total energy content, and the higher the cloud will rise. In some cloud models, mainly those in one dimension, entrainment is explicit (see, e.g., Simpson et al., 1965). In these models the height of rise of the simulated cloud is controlled by specifying the cloud radius, and consequently the rate of entrainment. In the cloud-simulation model used here entrainment cannot be controlled directly because it is implicit. However, the radius of the calculated cloud can be controlled to some extent by adjusting the horizontal dimension and intensity of the perturbation that initiates convection, and this in turn implicitly affects the height of rise of the cloud top.

In the present experiment, Cloud A rose to 5.8 km, evidently reflecting moderate entrainment. Some natural clouds in the area at which the sounding was taken (Puerto Rico on 20 August 1963) were of about that height, but a few grew larger, and many more smaller ones were also present (see Figs. 5 and 7 of Simpson et al., 1965). Thus, the simulation must be considered as realistic, at least as regards cloud-top height. Whether it should be considered as a "median" or "typical" cloud cell with regard to energetics is an open question, but a reasonable argument could be made to that effect.

The specific static energy change caused by the development of Cloud A is shown in Fig. 12. Both changes along the cloud axis and throughout the domain are given. The upward movement of energy is clear, particularly in the region of active cloud growth. The large increases in the upper half of the cloud are due largely to increased latent enthalpy. At these levels there is little change outside the cloud (Fig. 7), but there is an average increase for the entire domain because of the in-cloud contribution. Near the level of the cloud summit but away from the cloud there is some increase in water vapor, as can be seen in Fig. 3; but outside the cloud, at the height of its lower part, there is sufficient loss of water vapor that the static

energy change for the domain goes negative, although it is still posi-
tive for the cloud axis (Fig. 12). The increase in vapor near the
ground several cloud radii away from the axis causes the loss of static
energy in the entire subcloud layer to be less than that in the same
layer near the cloud itself. This latter loss is, again, primarily
due to loss of latent enthalpy (water vapor). Thus, in general the
latent enthalpy term dominates the static energy change, and conse-
quently it dominates the contribution of the convection toward stabiliz-
ing the atmosphere.

There are other important effects, however, in addition to changes
in latent enthalpy. In particular, the potential energy increases near
the cloud and decreases in the outer regions. The latter changes are
particularly important in relation to changes in other types of energy,
which are much smaller in that region.

It is clear that this single cloud does not stabilize its environ-
ment greatly, although the tendency is certainly in that direction.
According to Fig. 11, for the atmosphere to achieve neutral stability
(static energy independent of height) it is necessary to decrease the
static energy below 3 km by an average of about 10^4 J kg^{-1} and increase
the static energy above that level by a like amount. When summed over
a cylinder of 6 km radius and 3 km depth, with appropriate air density,
this amounts to about 3×10^{15} J.

In the present experiment, the loss sustained between the ground
surface and 3 km, determined by adding slab-summed differences, was
only 1.2×10^{13} J. A cross-check on this value can be obtained by
noting in Table 2 that the total condensate of 3558 metric tons repre-
sents a latent enthalpy of $3.558 \times 10^6 \times 2.5 \times 10^6$, or nearly 9×10^{12} J.
Since these two values are in reasonable agreement, they inspire con-
fidence in the validity of the calculations. It follows that the
energy rearrangement was about one-half of one percent of that required
to achieve neutral stability.

If this experiment had shown full stabilization, however, it would
have been unrealistic, for in nature such stabilization is achieved not
by a single cloud tower but an ensemble of clouds. At the height of
its vigor, Cloud A occupied a horizontal area of about one percent of

its computational domain, and the rest of the area was cloud-free.
This is a rather low ratio for cloudy area to clear area, as many
observations show, in particular those of Simpson et al. (1965). It
was mentioned earlier in this discussion that the annulus of air from
3 km to 6 km radius is not greatly affected by the cloud, but there
is a zone of decreased low-level stability at a radius of about 3 km.
This suggests that favorable conditions exist for additional convective
activity at this range. Since the area of the domain beyond 3 km is
4 times that within 3 km, a case can be made that the area controlled
by a convective cell of this size is about one-fifth the area of this
computational domain, so that in nature about 5 centers of convection
would occur in a domain of this size. The geometry of the model pre-
cludes the appearance of these additional convective centers in the
simulation. This supposition of a natural domain does not conflict
with observations of cloud density, although it is true that a tall,
vigorous cloud can depress convection in its immediate vicinity.

Another consideration is that Cloud A is not really representa-
tive of a natural cloud but more nearly resembles a cloud tower. Clouds
of this depth (5 km) normally consist of more than one tower, perhaps
four or more. Observations from aircraft suggest characteristic active
lifetimes of 15 minutes per tower. Thus we estimate that typically
about 20 times as much convection would be occurring in this domain as
is simulated. If so, then in one hour about 10 percent of the total
rearrangement required to achieve neutral stability would be accomp-
lished. According to this interpretation, the collective effect of
convection will, because of the interactions between clouds, result in
a vertical rearrangement lying somewhere between the "on-axis" and
"domain" patterns shown in Fig. 12. That is, the entire subcloud layer
will lose energy, and the region of greatest addition of energy will
be somewhat below the region of minimum specific energy.

Clouds with a larger volume-to-surface ratio than the model cloud
would suffer less relative mixing; therefore they would be deeper and
more energetic. The loss of energy in their lower regions and in the
subcloud layer would also be greater. Such clouds would be more effec-
tive than the cloud modeled in transporting energy upward, and conversely
smaller clouds would be less effective.

The deeper clouds are required if energy is to be transported to the higher levels. However, under normal trade-wind conditions the larger clouds are few in number, and it is not obvious whether the more numerous but individually less effective small clouds or the rare but individually more effective large clouds contribute more to the ultimate rearrangement of energy in levels of the atmosphere occupied by both.

It should be noted that the rearrangement of energy and the degree of stabilization of the atmosphere is not governed by the amount of rainfall that occurs. A non-raining cloud will still cause a rearrangement of the vertical distribution of energy in the atmosphere. In the model cloud the amount of rainfall is an order of magnitude less than the total condensation, and it is the redistribution of water vapor through condensation, advection, and evaporation that has the greatest effect. In the case of Cloud A, the enthalpy lost from the atmosphere by the fallout of rain (thermal enthalpy of water removed from the system) was half the change in latent enthalpy and much less than the changes of either thermal enthalpy of the atmosphere or potential energy; see Table 2. The product of the mass of water rained out and the latent heat of condensation is equal to the loss of latent enthalpy by the atmosphere.

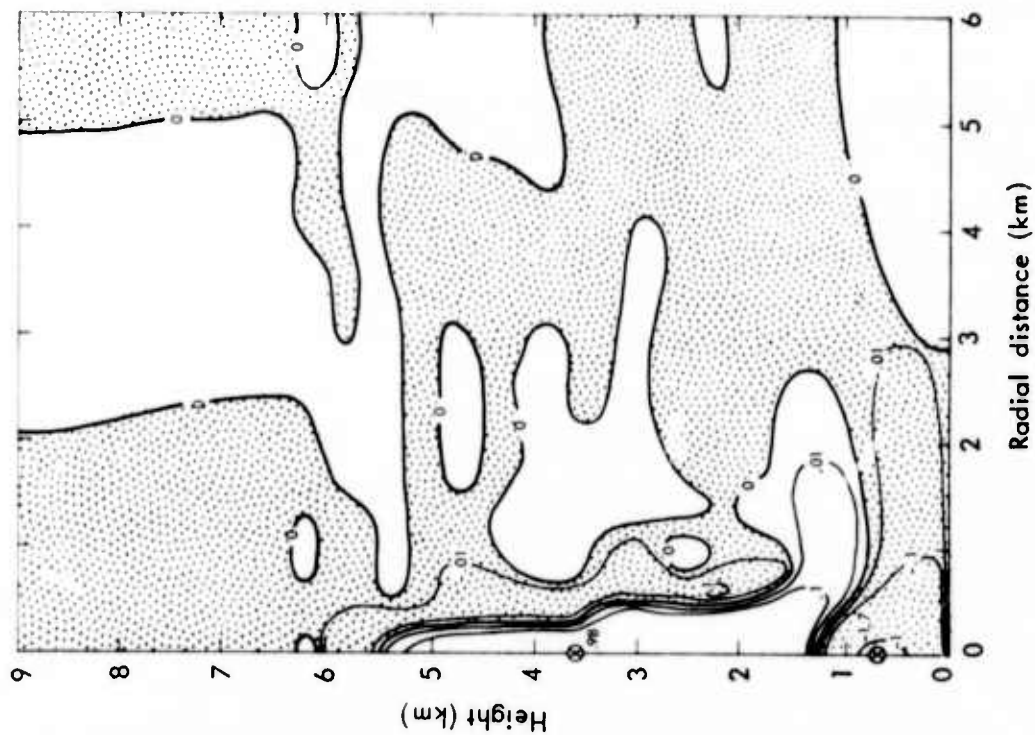## V. ENERGY TRANSPORT

ENERGY FLUX

The flux of various quantities is closely related to the wind field. The patterns of time-averaged winds, $\tilde{u}$ and $\tilde{w}$, provide a general picture of the horizontal and vertical movement of the air and consequently of the energy transport. These fields, for Cloud B, are shown in Figs. 13 and 14. The strong upward movement of air within the cloud (reaching a maximum of nearly 1 m s^{-1}) and the strong downward movement beneath the cloud (1.7 m s^{-1}) are conspicuous. The mean wind in the subcloud downdraft achieves larger values than the mean wind in the updraft because of its consistency of direction rather than its maximum instantaneous strength.

The mean horizontal wind pattern shows inflow toward the cloud in the subcloud layer except for a region of strong outflow in a shallow layer near the ground associated with the deflection of the downdraft by the rigid boundary. A maximum of nearly 1 m s^{-1} is reached in this region. Near the cloud top the outflow and inflow are characteristic of the ring vortex which the cloud circulation to some extent resembles. Air movement around the midsection of the cloud is not well defined in the mean. This is due to the fact that air at a given height first moves outward as the cloud top approaches from below, then inward as the cloud top moves through the zone; consequently, the horizontal wind components tend to cancel each other in the process of time averaging, and no clear pattern of mean wind flow results.

In computing energy flux, no account was taken of the changes in the form of energy that might be occurring simultaneously. Hence, conclusions based solely on flux data may not be supported by data discussed in Sec. IV regarding the overall changes in energy.
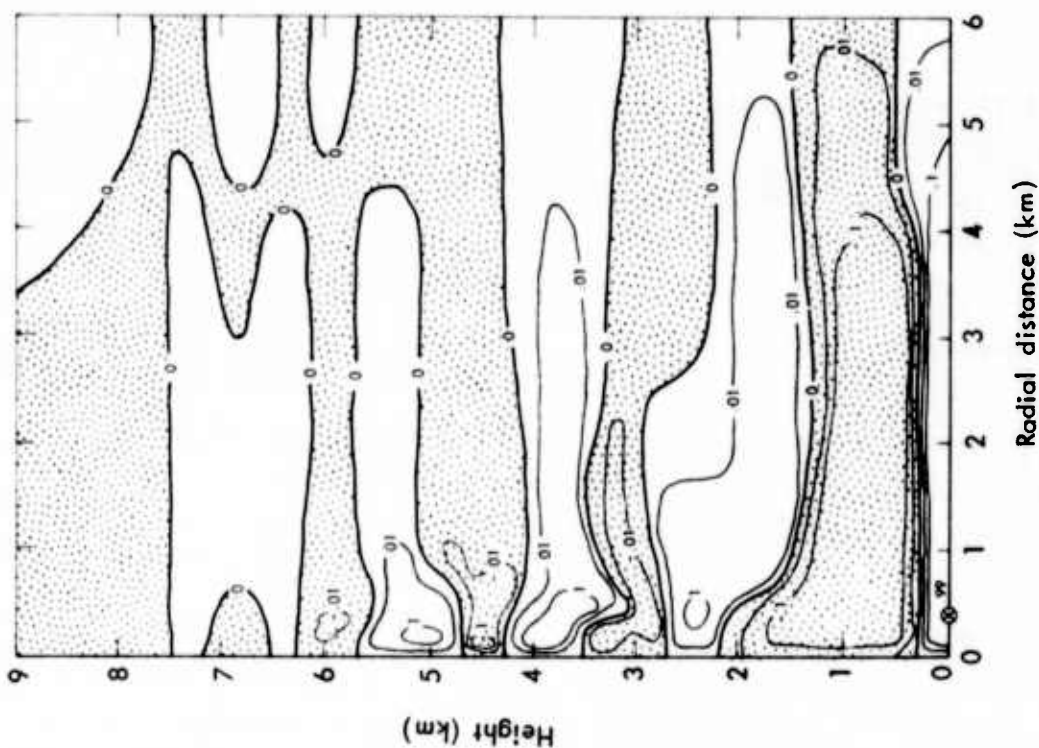
LATENT ENTHALPY FLUX

The flux of latent enthalpy averaged over a period of one hour is shown in Fig. 15. The strong upward movement of energy, related to moisture, near the cloud base and extending through the cloud volume,

NOTE: Shaded area represents downward motion. Field maximum and minimum are designated by the symbol ⊗, with values alongside.

Fig. 14—Average vertical wind components (m s^{-1}), 0 to 60 min, Cloud B

NOTE: Shaded area represents inflow toward axis. Field maximum is designated by the symbol ⊗, with value alongside.

Fig. 13—Average horizontal wind components (m s^{-1}), 0 to 60 min, Cloud B

is clearly shown. In the cloud region the size of the term $\widetilde{w''\eta_L}''$ (not illustrated) is about one-third the total average flux, whereas away from the cloud this term is orders of magnitude smaller than the total average flux. Thus the correlation between the departures of vertical wind and latent enthalpy, which is high within the cloud and low away from the cloud, is clearly indicated. The horizontally summed average flux of latent enthalpy $\langle AF_L \rangle$ is shown in Fig. 19(a). There is vertical divergence throughout a layer extending from near the ground up to 1.8 km. Above the height of the cloud base (near 1.2 km) latent enthalpy flows upward, and below this level it flows downward.

The center of latent enthalpy moves downward, as indicated in Fig. 20, suggesting an overall downward motion of water vapor throughout the domain over the lifetime of the cloud. The general subsidence in the outer reaches of the domain and the rain shaft apparently carry more water vapor downward than the active convection carries upward. This overall movement of moisture is unexpected, for cumulus convection normally is thought to cause the transport of moisture upward. This matter was further examined by finding the height at which half the water vapor in the atmosphere lay above and half below. Initially, this height was 1310 m. At 60 sec, it had descended a mean distance of 10 cm throughout the entire domain, but on the cloud axis itself it had ascended 22 m. These values take into account both the transformation (to rain) and the advection of water vapor, and they corroborate the flux values. There is reason to suspect that the fixed boundary and the geometry of the simulation is causing an unrealistic amount of downward flow in the outer region of the domain, thus causing the net downward flux of moisture. Following a similar argument developed in the discussion of environment stabilization, if additional clouds were present, the overall transport probably would be upward.

THERMAL ENTHALPY FLUX

The flux of thermal enthalpy is shown in Fig. 16. The pattern and magnitude of the flux are similar to that of latent enthalpy. The contribution of the $\widetilde{w''\eta_E}''$ term (not illustrated) is about 1 percent of the total flux near the cloud volume and diminishes to about 0.01 percent

in the middle of the computational domain. Thus, unlike the latent enthalpy flux, there is little correlation between the departures from the mean of the vertical motion and thermal enthalpy.

The horizontally summed fluxes of thermal enthalpy of dry air, water vapor, and condensed liquid are shown, respectively, in Figs. 19(b), 19(c), and 19(d), and their sum is shown in Fig. 19(e). Flux for the gas phases changes sign at the level of the cloud base, but for the liquid phase this occurs at a somewhat higher level. The absolute value of the flux of dry air enthalpy is an order of magnitude larger than that of water vapor which, in turn, is an order of magnitude larger than that of the liquid condensate.

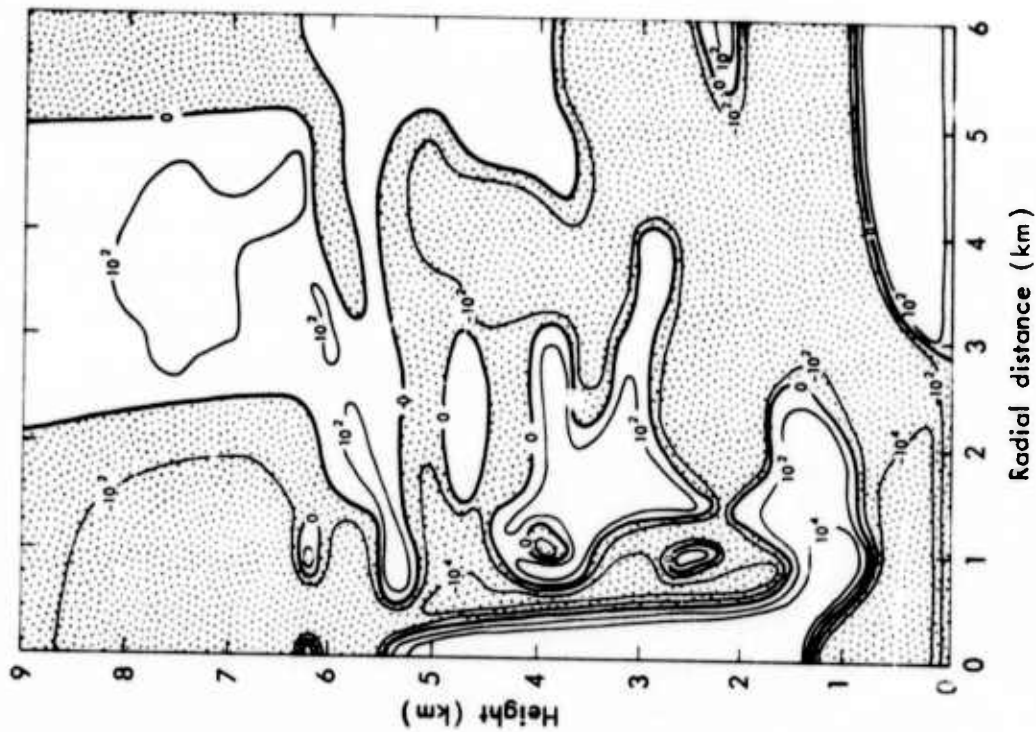The center of thermal enthalpy moves downward (Fig. 20).

POTENTIAL ENERGY FLUX

The flux of potential energy is shown in Fig. 17. Again, the pattern and magnitude are similar to those of latent enthalpy, but, as in the case of thermal enthalpy flux, there is relatively little correlation between the departures of vertical wind and potential energy. Immediately above the cloud there is a slight downward flux in potential energy occasioned by subsidence, which is indicated in Fig. 14.

The horizontally averaged potential energy flux is shown in Fig. 19(f). The relatively small downward flux at the bottom of the domain and the disproportionately large upward flux within the cloud compared with those of latent and thermal enthalpies are due to the height dependence of potential energy, which is much stronger than that of enthalpy and generally of opposite sign.

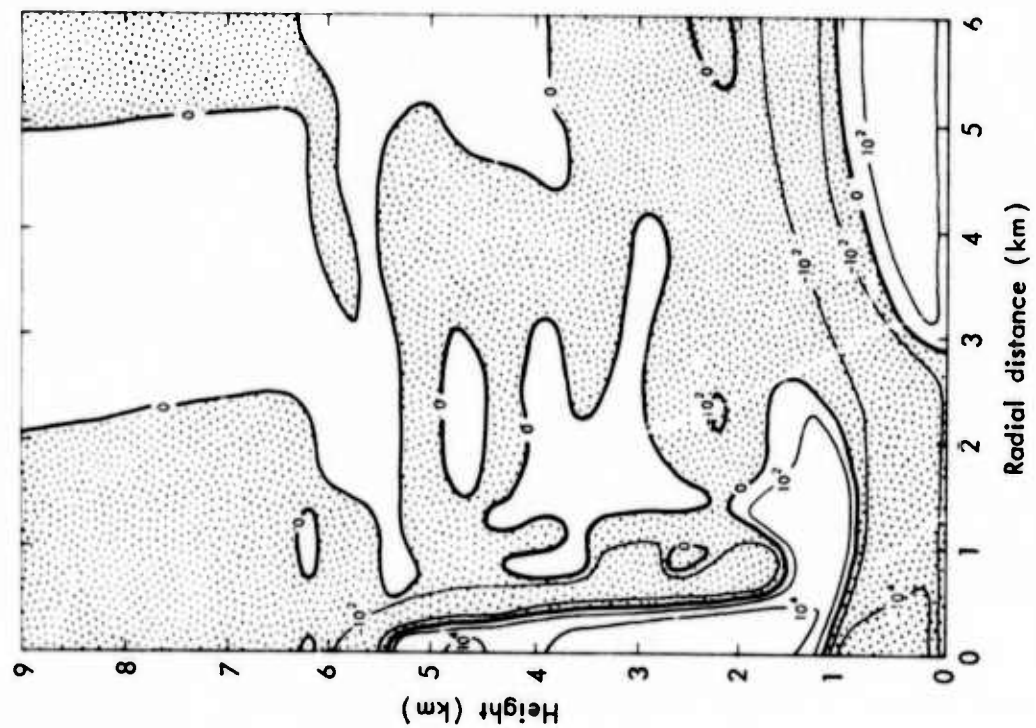The center of potential energy moves upward (Fig. 20).

STATIC ENERGY FLUX

The flux of static energy is shown in Fig. 18. It equals the sum of the potential energy and thermal and latent enthalpy fluxes and shares their characteristics. Within the cloud volume $\widetilde{w''\eta_s''}$ is about 10 percent of $\widetilde{w\eta_s}$, whereas elsewhere in the domain it is 0.1 percent of $\widetilde{w\eta_s}$. That is to say, vertical wind and static energy are slightly
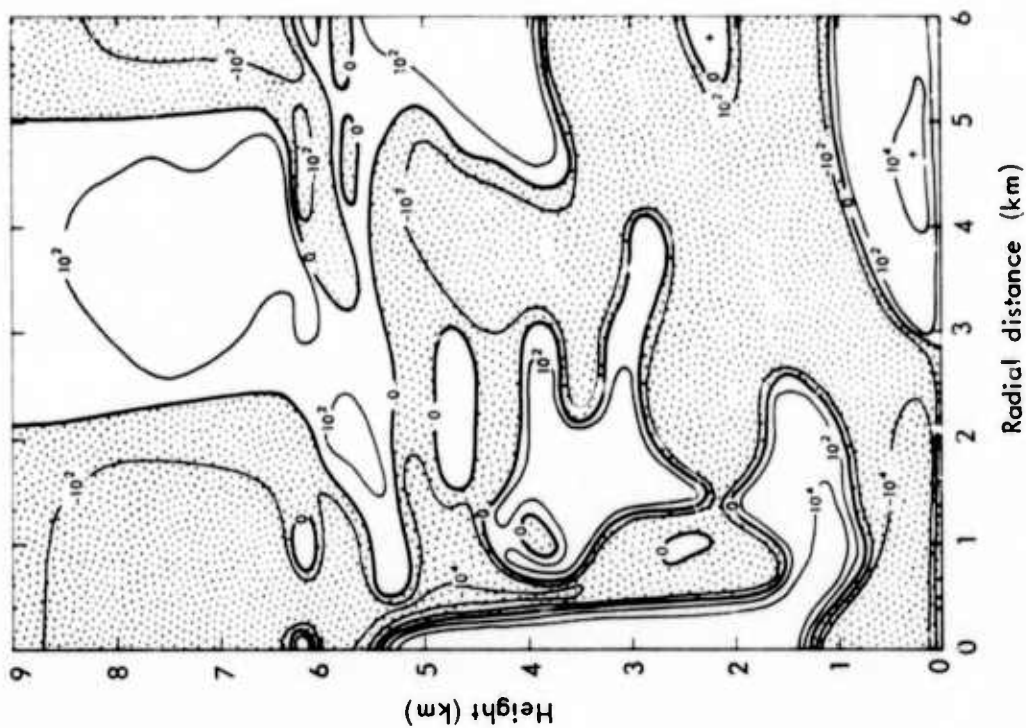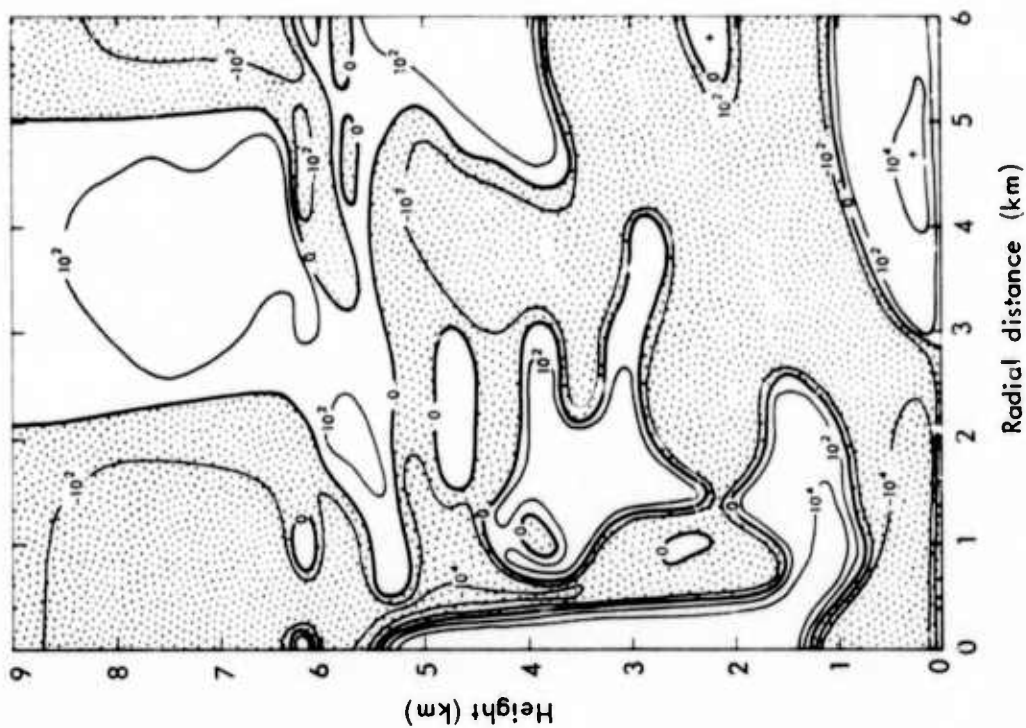
NOTE: Shaded area represents downward flux.

Fig. 16—Average vertical flux of thermal enthalpy
(J m⁻² s⁻¹), Cloud B

NOTE: Shaded area represents downward flux.

Fig. 15—Average vertical flux of latent enthalpy
(J m⁻² s⁻¹), Cloud B

NOTE: Shaded area represents downward flux.

Fig. 18—Average vertical flux of static energy
(J m⁻² s⁻¹), Cloud B

NOTE: Shaded area represents downward flux.

Fig. 17—Average vertical flux of potential energy
(J m⁻² s⁻¹), Cloud B

-54-
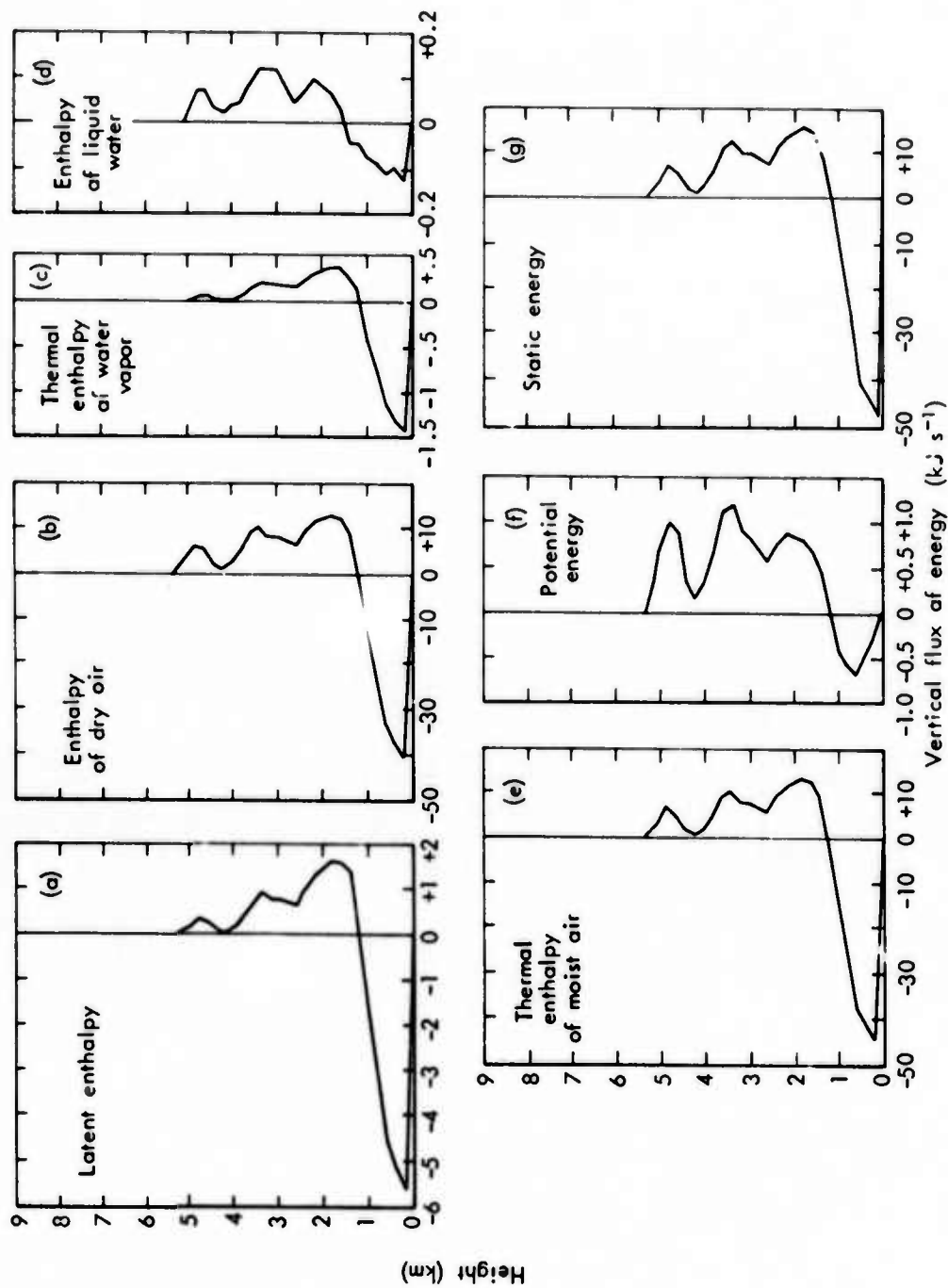
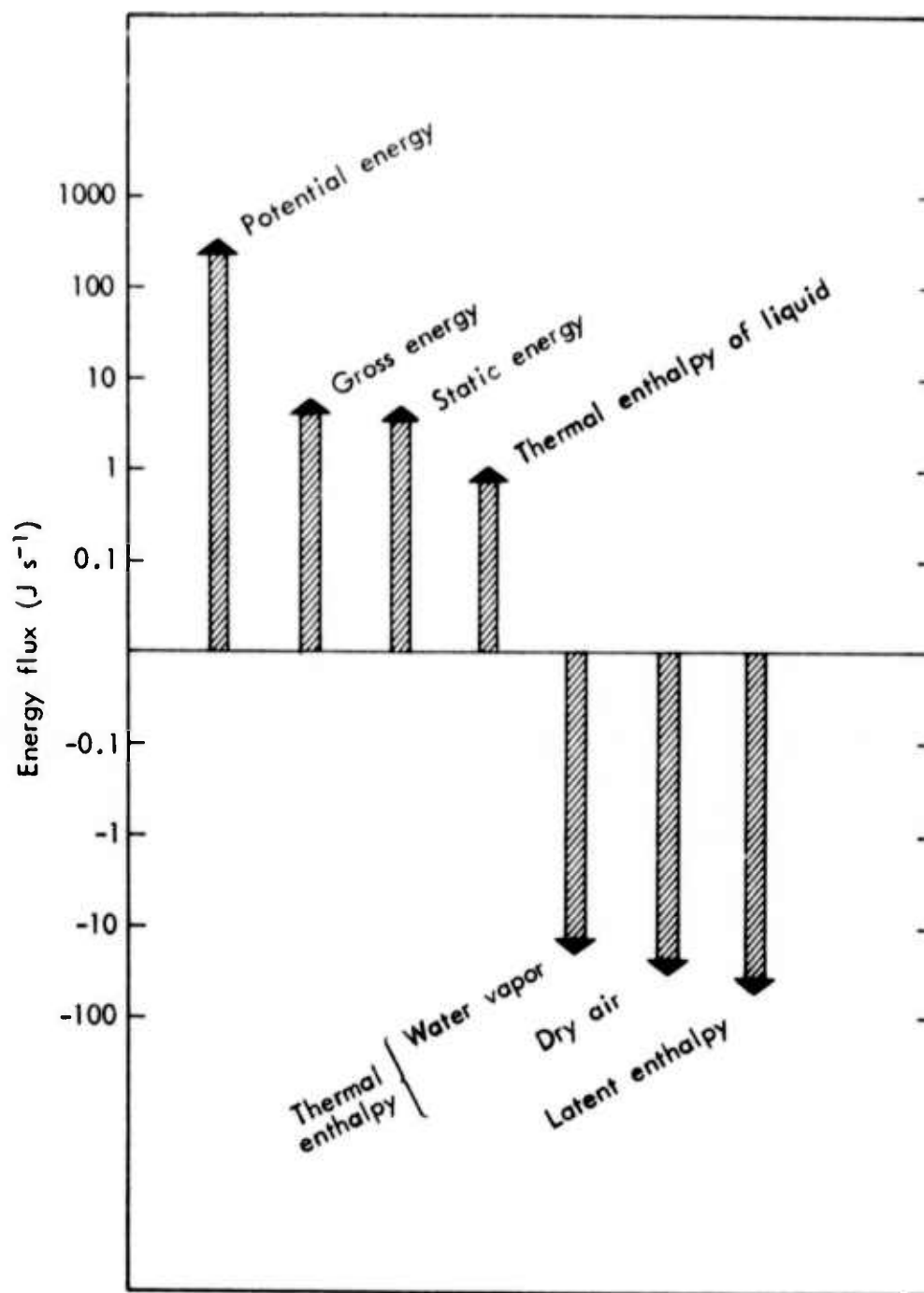Fig. 19—Average vertical flux summed by slabs (KJ(36π km²)⁻¹ s⁻¹), Cloud B

Fig. 20—Vertically averaged vertical flux of energy of various categories, Cloud B
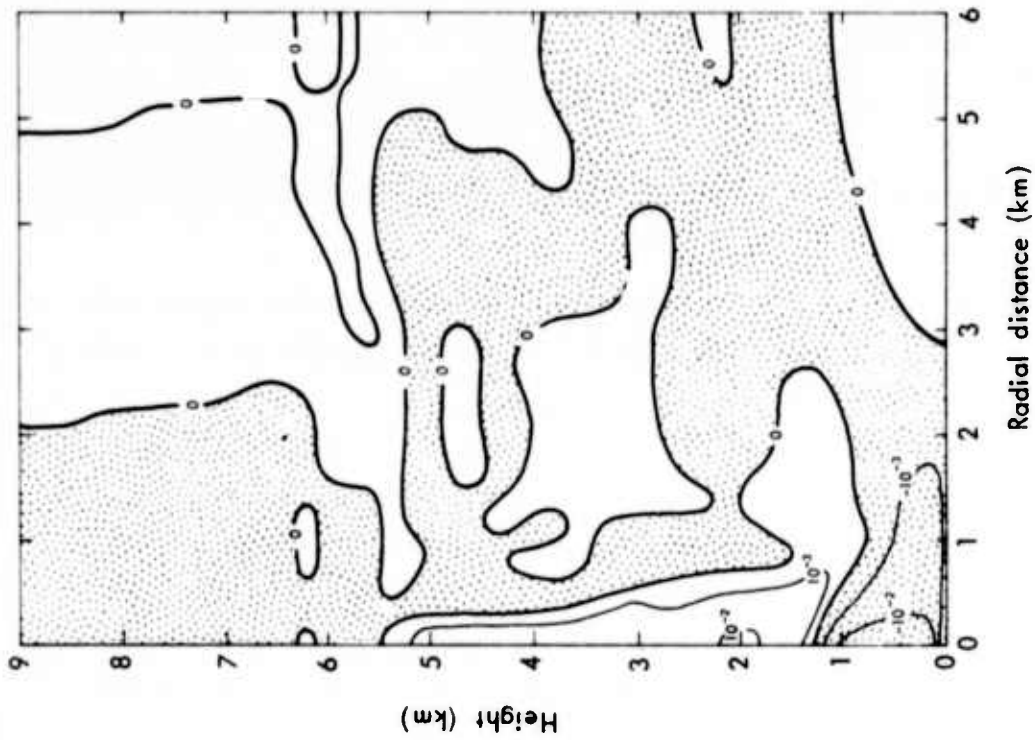
correlated in the region of maximum convective activity and hardly correlated at all elsewhere.

The largest component of the static energy flux is the thermal enthalpy of dry air. This reflects the large mass of air involved in the flow field in comparison with the mass of water substance. The net flux of dry air enthalpy is close to zero, however, and the upward movement of the center of static energy (Fig. 20) largely reflects the consistent upward flux of potential energy.
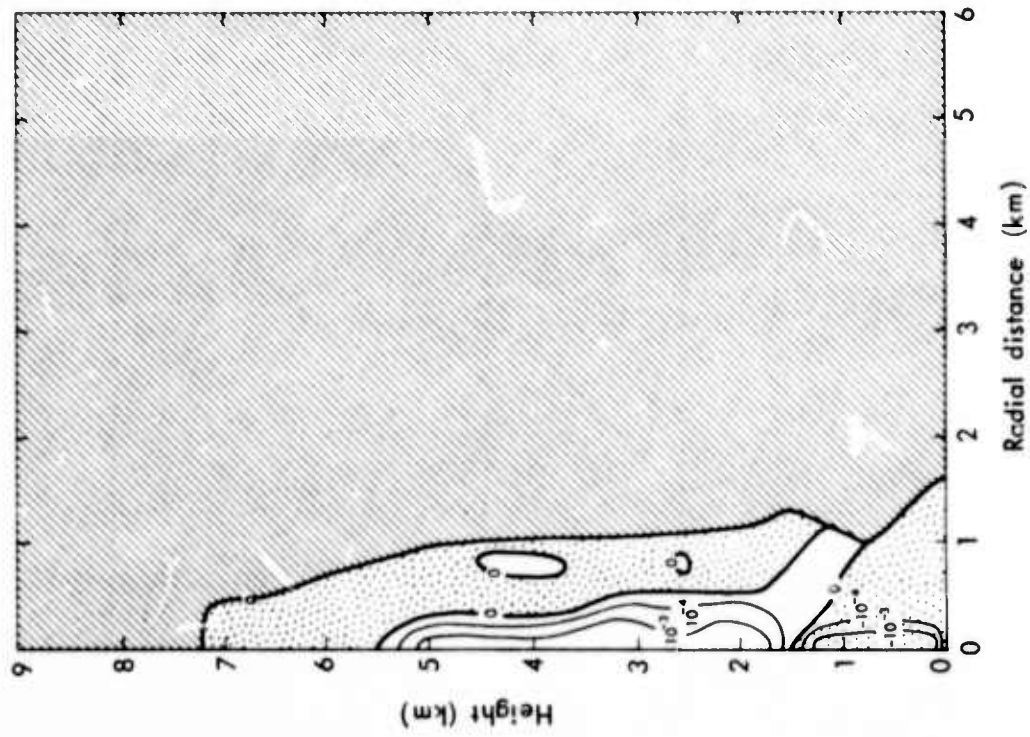
FLUX OF WATER SUBSTANCE

Since some of the major forms of energy depend critically on the amount of water vapor or liquid condensate contained in the air, it is instructive to see how these constituents are transported. Figure 21 shows the vertical flux of water vapor, and Fig. 22 shows that of liquid condensate. The familiar pattern of the mean vertical wind is apparent in the former. The latter is zero over most of the domain because of the absence of cloud in those regions. The area of downward flux above 5.5 km and to the side of the cloud is associated with very small amounts of water carried above the nominal cloud top by eddy diffusion, which enters both implicitly through the differencing algorithms and explicitly.

The horizontally summed flux values for water vapor and total water substance (vapor plus condensate) are shown in Fig. 23. The large downward flux of vapor near and below the cloud base (1200 m) is attributable to the downdraft beneath the cloud as well as subsidence in the environment away from the cloud. The predominance of the vapor phase with reference to the transport of water substance is clearly evident in the lower part of the domain, but near the cloud top the condensed phase accounts for about half of the flux. Part of the reason for this is that the upward flux of vapor within the cloud at a given level is offset to a degree by the downward flux outside the cloud at the same level. Also, vapor content decreases with increasing altitude throughout the domain, but over much of the region occupied by the cloud the liquid content is more or less independent of height.

NOTE: Shaded area represents downward flux. Hatched area represents zero flux due to absence of liquid.

Fig. 22—Average vertical flux of liquid water (kg m^{-2} s^{-1}), Cloud B

NOTE: Shaded area represents downward flux.

Fig. 21—Average vertical flux of water vapor (kg m^{-2} s^{-1}), Cloud B
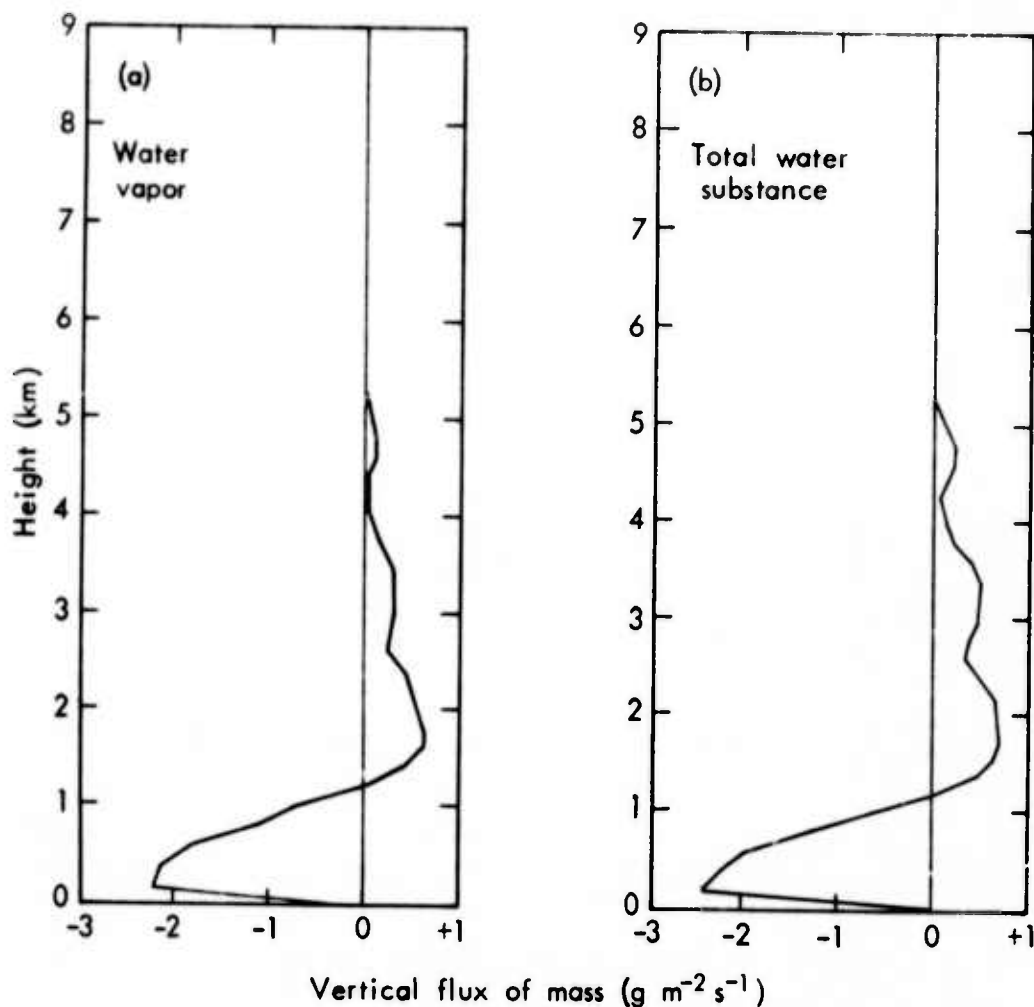
Fig. 23—Average vertical flux summed by slabs (g m^{-2} s^{-1}), Cloud B

It should be noted that the flux calculation for the liquid water does not take into account the gravitational fall of the larger drops with respect to their associated air parcels.

FLUX DIVERGENCE

The vertical divergence of several categories of energy may be estimated from Fig. 19. Wherever a curve in that figure slopes upward to the right divergence is indicated, and wherever it slopes upward to the left convergence is indicated. This is more clearly shown in Fig. 24, which is based on the application of (3-41) to static energy. In effect, the curve in Fig. 24 is the derivative of the curve in Fig. 19(g).
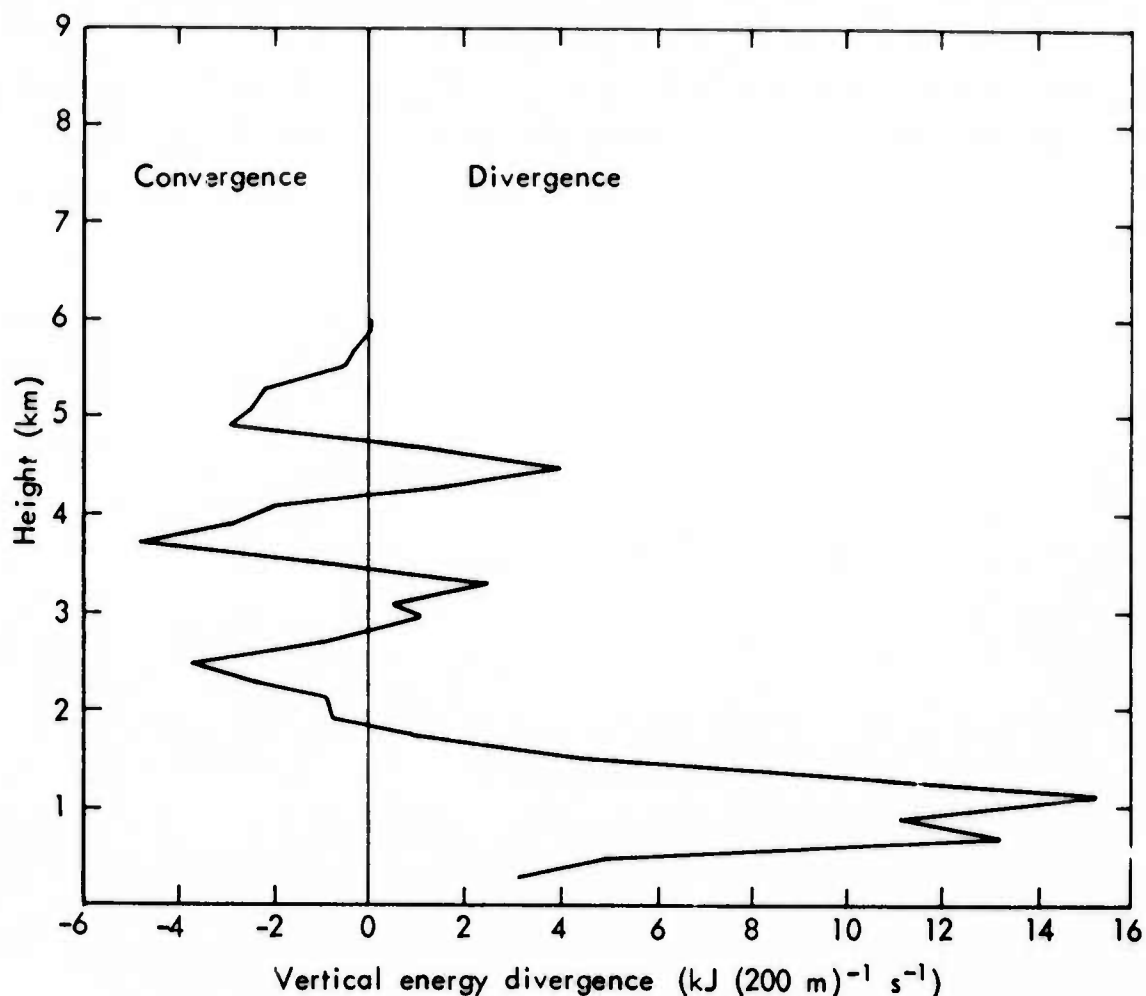
Fig. 24—Average vertical divergence per slab of static energy (KJ (200 m)$^{-1}$ s^{-1}), Cloud B

It is seen that static energy diverges from a region extending from near the ground surface to a level several hundred meters above the cloud base. The level of maximum divergence is at cloud base. At higher levels divergence alternates with convergence, but convergence predominates. The saw-tooth pattern of alternating positive and negative regions of divergence in Fig. 24 is associated with a similar variation of q_v with height in the original sounding. This is apparent in the dew-point curve of Fig. 1. This irregularity was the reason that the smoothed version of the sounding was used for much of this work.

The various categories of enthalpy and the potential energy that make up the static energy all have patterns of divergence similar to that shown in Fig. 24. The contribution of the enthalpy of dry air, however, is by far the largest.

VI. DIFFICULTIES--POTENTIAL AND REALIZED

We believe that some comments on problems that often occur in studies of this type, or that occurred during the course of this work, would be valuable in guiding future efforts and provide a feeling for the validity of these results.

ACCURACY OF DIFFERENCES

Energy and mass differences calculated before and after the exist- ence of a cloud constitute one of the principal quantitative outputs. Often, energy contents were large compared with differences. This suggests problems concerning the significance of the computed differ- ences. A check revealed that the simple subtraction of "before" and "after" values of all quantities was accurate to at least two decimal places. This is probably satisfactory for many purposes, but not for all; consequently, accuracy was substantially improved by calculating differences based on perturbations from a reference state, i.e.,

$$\Delta \phi = \phi_\tau - \phi_0 = (\overline{\phi} + \phi'_\tau) - (\overline{\phi} + \phi'_0) = \phi'_\tau - \phi'_0 = \Delta \phi' \qquad (6-1)$$

Except for the kinetic energy of an atmosphere starting at rest, the reference value, $\overline{\phi}$, will usually be large compared with ϕ'_τ or ϕ'_0. Hence, the accuracy of the differences was substantially increased by removing the large reference values and operating with the residues. Another device used to increase the significance of the differences was the factoring out of large constant quantities such as gz, L, or the coefficients of specific heat (see Sec. III). It is believed that sufficient care was thereby taken that the error arising from taking small differences of large quantities was negligible.

REARRANGEMENT OF ENERGY CAUSED BY THE FINITE-DIFFERENCE SCHEME

Normally, the cloud model has been run using real atmospheric soundings; consequently, there are nonsmooth transitions in the vertical. The finite-difference scheme used in the computations and the explicit

eddy diffusion terms that appear in the model's equations both tend
to smooth out these sudden transitions of water vapor content or temp-
erature. Hence there is a tendency for rearrangement of energy (in
this case, transport of thermal enthalpy and latent enthalpy without
transformation) to occur regardless of the presence or absence of
cumulus convection. This smoothing, which can be significant in com-
parison with that caused by convection, appears as large movements
from one layer to an adjacent layer across the entire horizontal
extent of the domain. It is distinguishable from convective motion,
which will have a much greater variation in the radial direction as
well as a more consistent and smooth transition in the vertical.

Figure 25 illustrates how effects caused by convection can be
obscured when the initial sounding is not smooth. At initial time
for Cloud B, the static energy summed by slabs had alternating
shallow layers of relatively large and small value resulting mainly
from large vertical gradients of humidity in the original unsmoothed
sounding. Subsequently, numerical smoothing introduced strong nega-
tive changes at levels of excess relative to adjacent grid levels,
and strong positive changes in regions of deficit relative to adjacent
grid levels, resulting in the saw-toothed curves of Fig. 25. This
problem may be reduced by using a smoothed sounding, as was done for
Cloud A.

Comparison of Fig. 8(g) for Cloud A with Fig. 25 for Cloud B shows
that the use of a smoothed sounding not only produces a smoother curve
of slab-summed energy change versus height, but also reduces the change
for a given slab by an order of magnitude or more. In this connection,
however, it should be noted that even the large changes of Fig. 25
represent only 1 percent of the basic values. Furthermore, the posi-
tive and negative changes tend to counterbalance each other, so the
total change cannot be too far off the mark, at least in a relative
sense. Nevertheless, the results with the smoothed sounding inspire
greater confidence.

REARRANGEMENT OF ENERGY CAUSED BY EDDY DIFFUSION

Usually, cloud dynamics models employ an eddy diffusion term in
most or all of the prognostic equations. Its purpose is to account for
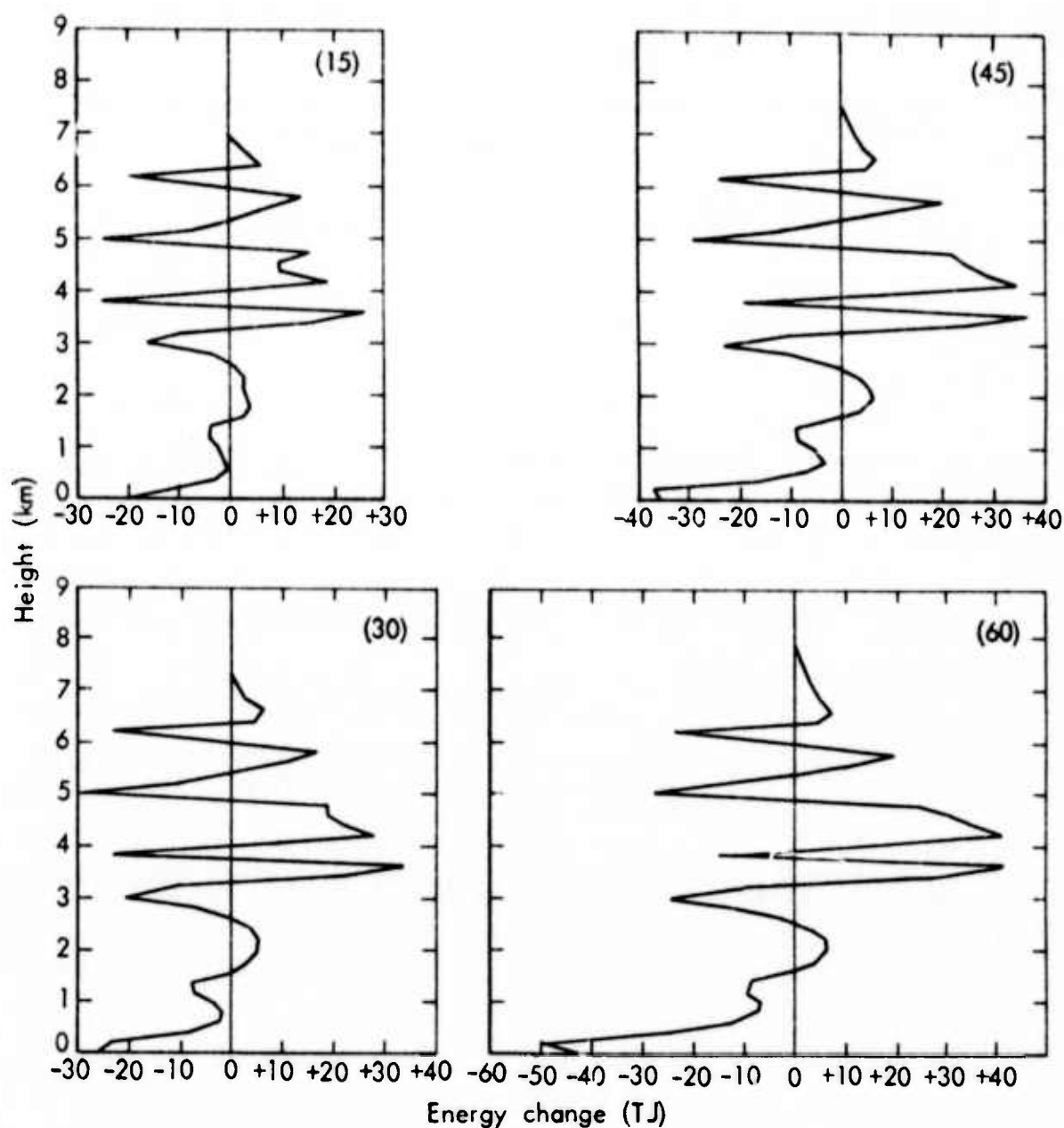
Fig. 25—Change from 0 to 15 min, 0 to 30 min, 0 to 45 min, and 0 to 60 min in static energy summed by slabs, from the unsmoothed sounding used in Cloud B

scales of motion too small to be resolved by the finite grid. In this model the eddy diffusion terms have the form $\nu\nabla^2\phi$, where ν is the eddy diffusion coefficient and ϕ might be the momentum, temperature departure, or mixing ratio of a constituent. The effect of eddy diffusion, at least in this form, is to "smear" values even in the absence of a wind field.

Whether or not eddy diffusion is to be used is a matter of judgment that ultimately depends on whether the cloud simulation is more realistic with or without the term. We have not finally resolved this matter, but our best results seem to have come with the use of a coefficient of $\nu = 40 \text{ m}^2 \text{ sec}^{-1}$ applied to the momentum, temperature departure, mixing ratio of water vapor, and mixing ratio of the part of liquid that is in the form of small droplets and $\nu = 0$ to the part of the liquid that is in the form of large drops.

The model starts its computations with a specified atmosphere that is uniform in the horizontal. To induce convection some kind of perturbation must be introduced. The perturbation might be a horizontal gradient in the buoyancy in some limited region, which will induce motion, or it might be a field of motion itself. In both cases self-sustaining convection can be set off only by updraft sufficient to cause some condensation.

Normally, a buoyancy perturbation arising from altered humidity has been employed in using this model. It is a reasonable emulation of nature's methods of inducing convection (see Bunker et al., 1949, and Malkus, 1954), and it was used in the computation of Cloud B. It is equally reasonable to start with an initial field of motion; this was done in Cloud A.

Any perturbation amounts to a perturbation in energy. Because the initial state of the atmosphere includes the perturbation insofar as the energy calculations are concerned, some of the energy changes can be affected by the spread of that perturbation through numerical diffusion from the finite-difference scheme or through eddy diffusion. Even though the eddy diffusion terms represent real phenomena, their finite-difference implementation can cause the spreading of small quantities of the substance involved at speeds of one grid unit per time step, well in excess of any speed actually permitted by the model. This spreading, which is more apparent with a humidity perturbation than with a field of motion, can occur even in the absence of convection. And, as in the case of vertical irregularities in the basic sounding, the energy rearrangements occasioned by the spreading of the perturbation may be comparable in size to those caused by the

convection. Again, the problem is less serious with respect to flux calculations.

The phenomenon is illustrated in Fig. 26. The initial humidity perturbation had a maximum at the central axis and decreased to zero at 2 km radial distance. Artificial diffusion causes an unusually large transport of humidity outward across the edge of the perturbation, resulting in a cusp at 2 km in all the curves of Fig. 26.

To minimize this effect the energy of the perturbation should be minimal. The humidity perturbation contains large amounts of energy in the form of thermal and latent enthalpy; hence it is not optimum for this purpose. In the present experiment at least, kinetic energy is one of the smallest forms of energy in the atmosphere, and furthermore, if free convection is not initiated, kinetic energy is rapidly damped. It does affect the flux, however.

It was as a consequence of these considerations that Cloud A with a momentum impulse was used to analyze the energy changes and Cloud B with humidity impulse was used for the flux calculations.

COMPUTATION GEOMETRY

The computational domain is a cylinder with a vertical axis. It is described by cylindrical coordinates with a uniform mesh length D in the horizontal and the vertical. Axial symmetry is assumed, so each interior grid point represents an annulus of width and depth D and radius depending on the horizontal index of the grid point. (Boundary points are special cases.) It follows that the volume represented by a grid point varies with the square of the radial distance, and that small differences in energy density at large radial distances can assume great importance when summing.

Ideally, the computational domain should be so large that the atmosphere at the outer and upper boundaries is undisturbed by the convection. In this work the outer boundary is at 6 to 8 cloud radii, assuring relatively little disturbance, but permitting some. The increases noted toward the outer boundary in some of the graphs of Fig. 9 are probably the result of rather insignificant changes magnified by the effect of the square of the radial distance. Caution must be used in assessing the realism and significance of some of the results.
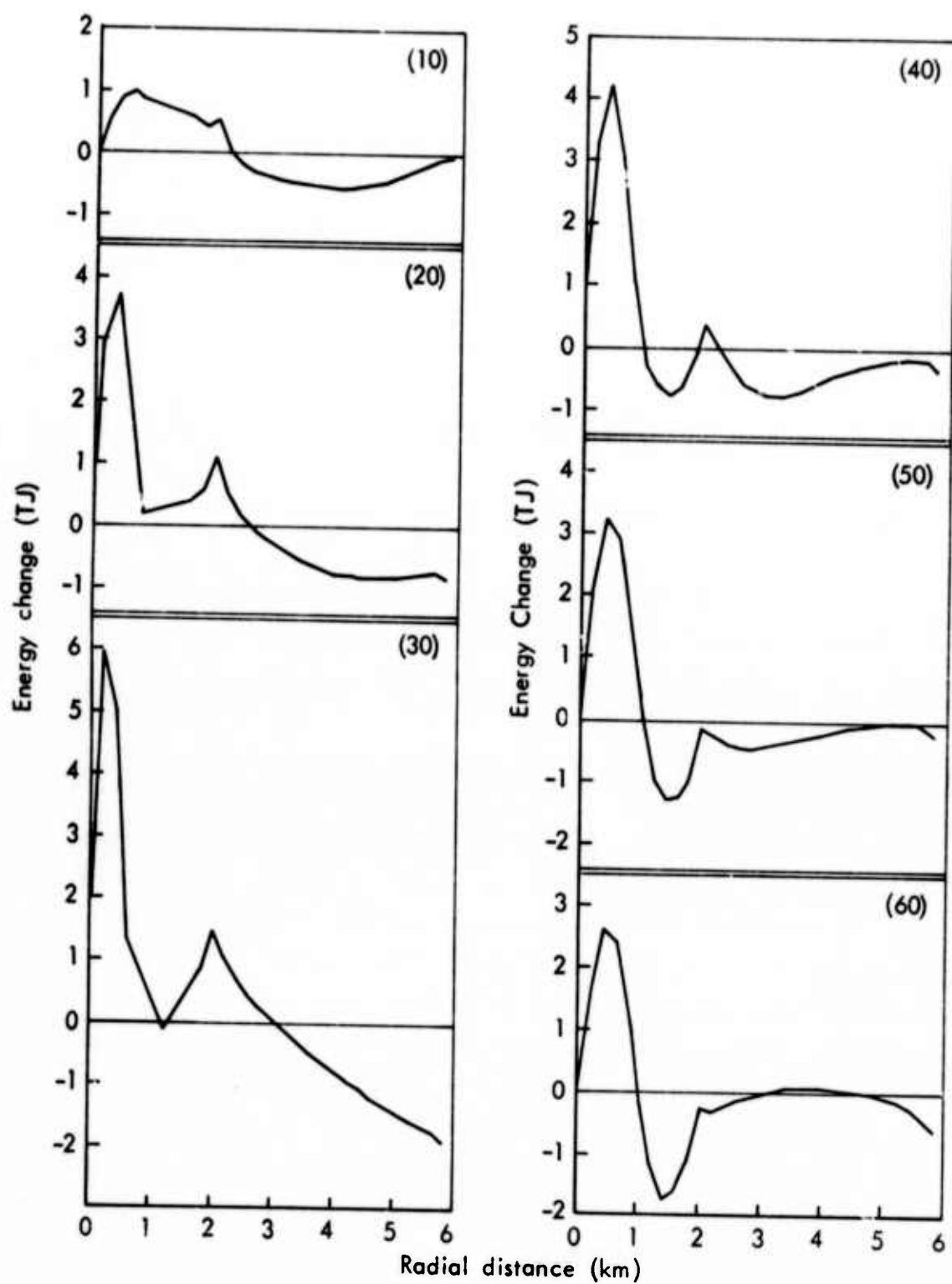
Fig. 26—Change from 0 to 10 min, 0 to 20 min, 0 to 30 min, 0 to 40 min, 0 to 50 min, and 0 to 60 min of static energy summed by tubes, from a run with a humidity perturbation

The geometry and resolution are such that the cloud top and side are well defined by the energy differences. All values show a sharp decrease across the cloud boundaries.

POTENTIAL ENERGY--AIR DENSITY IN A BOUSSINESQ MODEL

Since the cloud simulations on which this study of energetics is based come from a Boussinesq model, the expressions for the various types of energy should be formulated in a way that is consistent with the Boussinesq assumptions. In the present study this was done by deriving the energy equations (2-32) for unit mass of cloudy air and (2-40) for unit volume from the Boussinesq equation of motion. The outcome was that wherever air density enters it appears as a reference density dependent only on height, except that in the potential energy term the full current local density appears. In all cases the air density is dependent on the water vapor and condensed water content, but in the case of potential energy it is also dependent on pressure and temperature.

To evaluate (2-42), one must know the value of ρ, which in accordance with (2-10) is equal to $\bar{\rho} + \rho'$. The reference density is computed as a function of z once and for all at initial time. The density departure can be found with the use of the Boussinesq equation of state

$$\frac{\rho'}{\bar{\rho}} = \frac{p'}{\bar{p}} - \frac{T'}{\bar{T}} \tag{6-2}$$

The cloud model does not in principle require that p' be computed, for as a rule $p'/\bar{p}$ is at least an order of magnitude smaller than $T'/\bar{T}$. For some purposes, however, such as the present one, it is desirable to know the value of p'. This can be found by solving an elliptical partial differential diagnostic equation, or more simply, by solving the third equation of motion for $\partial p'/\partial z$ with dw/dt a known quantity from values of w at the beginning and end of the time-step, followed by integrating from the rigid lid of the computational domain (at which p' = 0) to the ground surface. The disadvantage of solving for pressure in this way is that the solution lags one time-step behind

the microphysical calculations, and so there is a potential for considerable error Since p' is so small anyhow, the error should not be troublesome.

In order to determine the importance of the complete air density value to the potential energy density, some calculations were made using $\bar{\rho}_a$ rather than ρ_a in (2-42). This is called a "constant density" situation because air density does not depend on the current temperature and pressure even though it varies with height and vapor and liquid content. As can be seen from Fig. 27, the pattern of change of potential energy using "constant" density closely resembles that of latent enthalpy (Fig. 3), but the values are several orders of magnitude smaller. This would lead one to conclude that changes in potential energy are small and relatively unimportant.

The results are significantly different, however, if potential energy density is computed with ρ_a in (2-42), as it should be, and with the use of (6-2); see Fig. 6. The absolute value of potential energy change is an order of magnitude larger than in Fig. 27, and although each figure shows a maximum in the vicinity of the cloud, they differ elsewhere.

Even though the use of variable dry-air density in computing potential energy is a more consistent application of the Boussinesq approximation than is the use of constant dry-air density, it still is not entirely satisfactory in the present formulation. Although the atmosphere should suffer a net loss in energy due to the removal of enthalpy of rain water, the loss shown by the present computation is seven times too large. This loss appears to be related to large decreases in potential energy occurring near the outer edge of the computational domain. This, in turn, is probably related to widespread subsidence resulting from continuity in a closed domain of arbitrary size. It is conceivable that the problem might be lessened if the model permitted the spacing between neighboring convective cells to be determined dynamically.

Also, when using variable dry-air density there is no assurance that the mass of dry air is conserved. If there is a loss in mass, there will be a loss in potential energy. This could account for the
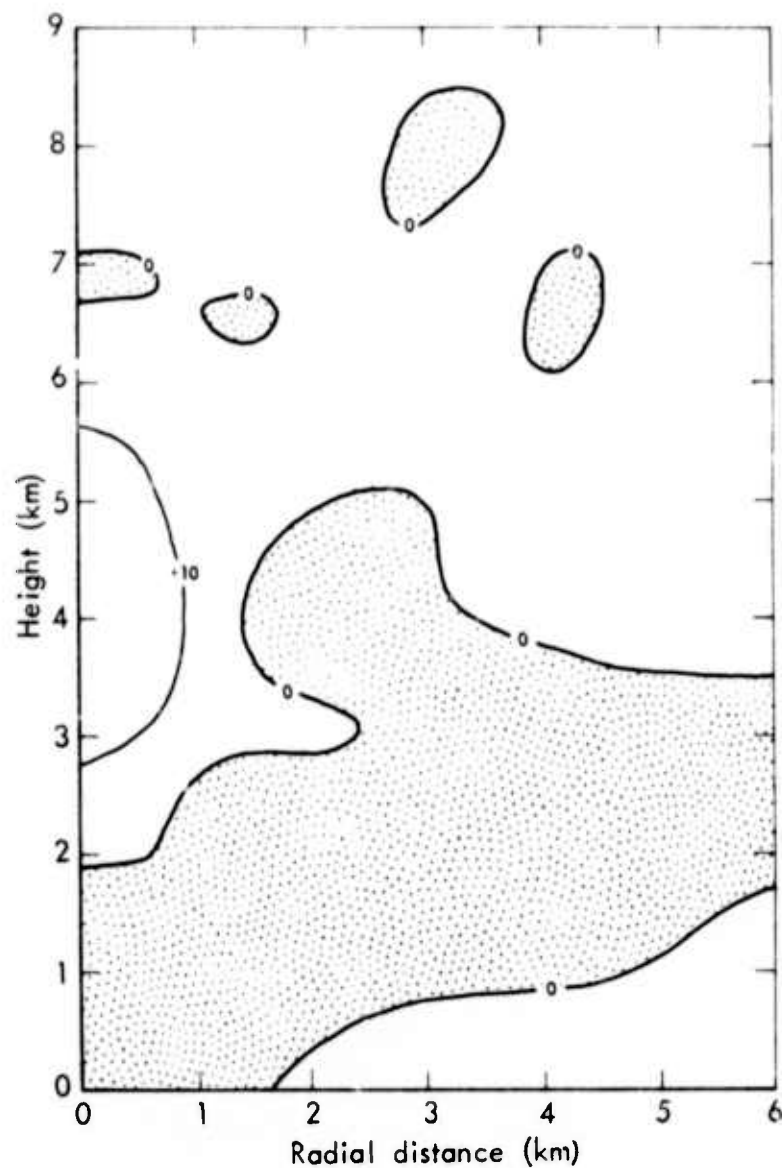
NOTE: Shaded areas represent a decrease.

Fig. 27—Change from 0 to 60 min of potential energy density $(J\ m^{-3}\ hr^{-1})$
using $\bar{\rho}_a(q_a + q_v + q_\ell)$ for total air density, Cloud A

apparently too large decrease in the potential energy of the domain.
The large region of Fig. 6 showing decreased potential energy density
with little radius dependence suggests an overall loss of mass. Per-
haps dry-air mass conservation should be accounted for in a manner
similar to that used to conserve water substance; this probably would
improve the energy balance.

VII. CONCLUSIONS

Although results from only two cloud runs are shown in the analysis, data derived from runs using other soundings or variations in some details of the model were available to supplement these data. Also, the numerical results generally support (i.e., compare favorably with) the analysis of Braham (1952) based on field observations. We therefore feel that our results warrant general interpretation--with reservations, of course.

This study involves the energetics of an isolated cloud tower. Most convection occurs with some degree of mesoscale (or even synoptic-scale) organization, and cells do not occur in isolation. How the transformation and rearrangement of energy is affected by the interference of superimposed effects is difficult to judge. The nature of the computational domain, a closed box, also limits the generalization that may be drawn. The effect of the domain is most apparent near the outer boundary, and unfortunately it is here that large masses of air are represented.

Another, perhaps more important, source of uncertainty in applying these results is the lack of balance in the energy summation. While the computations of total energy before and after convection agree to one part in 10^5, the fact remains that significant changes in the results could come about from changes in the distribution and form of that one part. We believe that if the computation were exactly conservative, the patterns of change would essentially duplicate those of this study. However, the vertical and horizontal summations might show important differences. Evidence suggests that the most questionable terms of the present computation are the potential energy and the thermal enthalpy of dry air.

FINDINGS PERTINENT TO CUMULUS PARAMETERIZATION IN MODELS OF LARGER SCALE

A finding of particular importance to the problem of parameterization of cumulus convection is that the energy available to stabilize

the atmosphere is equal to the total latent heat released during condensation (to generalize, include deposition) and not to the latent energy lost through removal of water from the atmosphere in the condensed phase as rain or snow. This confirms Braham's (1952) conclusions. He showed from data of the Thunderstorm Project that the latent heat of condensation of the liquid remnants of the cloud plus that of condensate that was re-evaporated considerably exceeds that of the rain that fell to the ground. Stated another way, it is hazardous to estimate (or parameterize) the amount of rainfall from the energy required to stabilize the atmosphere. Such an approach is basic to the general circulation model that has been used by Rand to model climate (Gates et al., 1971). Experience (Gates, 1972; Rapp and Warshaw, 1974) has shown that this model overestimates the amount of rainfall. From our analysis of cloud energetics, such an overestimate is to be expected. In effect, the rainfall parameterization assumes the cloud to have a precipitation efficiency of 100 percent (rain production equals total amount of condensation). By contrast, in the present calculation the precipitation efficiency was only 8 percent.

The present work, in agreement with Braham, suggests that the equivalent amount of condensate might be taken as the amount of heat required to stabilize the atmosphere and that the amount of rainfall should be a fraction of the total condensate (i.e., the condensate multiplied by the "cloud efficiency"). Cloud efficiency will vary with circumstances. The larger the cloud, in general, the greater the efficiency. Nominal values run between 0.25 and 0.75 approximately, but in certain climatic regions (e.g., the Southwestern United States) even large storms are observed not to produce rain at the ground because of substantial evaporation in the deep, dry subcloud layer.

Results of a run that used the initial conditions of Cloud A but did not permit precipitating drops to form suggest that nonraining clouds do not stabilize the subcloud region of the atmosphere. Instead, subsidence and downward transport of water vapor tend to increase the static energy below the cloud. The cloud layer itself, however, is stabilized. If this is true in nature, one would expect that small convective elements, probably "bubbles" of the type envisioned by Scorer and Ludlam (1953), would effect the stabilization

of the subcloud region. These convective elements would not necessarily result in condensation and would probably be below the limits of resolution of the present model. A cumulus model incorporating a good boundary-layer parameterization might demonstrate this process.

The present simulations suggest that the rate at which convective processes effect the adjustment of the atmosphere toward stability is slow, a period of the order of ten hours being required to decrease the instability to $1/e$ of its original value. This is in sharp contrast to the value of one hour used in the original version of the Rand climate model (Gates et al., 1971). The indication by the present cloud-model calculations that the rate of adjustment is slow is in accord both with general observations of convective activity and with Braham's (1952) conclusions.

FINDINGS REGARDING THE RELATIVE IMPORTANCE OF THE ENERGY TERMS

The kinetic energy involved in cumulus convection is negligible in comparison with static energy. The largest component in the static energy is the enthalpy of dry air. The latent enthalpy is about one order of magnitude smaller, but, because of the stratification of water vapor in the atmosphere and the involvement of water vapor in the cloud-forming process, the latent enthalpy term is much more variable in time and space and therefore accounts for the majority of the observed changes in energy. The water-vapor thermal enthalpy term generally varies with latent enthalpy, but is about one-fifth its value.

The potential energy term is important, particularly in locations away from the immediate vicinity of the cloud. The overall loss of potential energy is related to the large volume of subsiding air in the outer part of the domain. If there had been five convective elements in a domain of this size (a reasonable number, as has been previously indicated), this loss presumably would have been much diminished.

FINDINGS REGARDING THE LIFE CYCLE OF CONVECTIVE ELEMENTS

During the active, growing period of the cloud essentially all the condensate that is to form is produced. Thus the energy used for atmospheric stabilization becomes available during this time. Since the end

of the growing phase signals the end of new energy production, a rapid
decline in the energy available for rearrangement is experienced as
evaporation continues. In the runs used for this study, the cloud
reaches maturity, and nearly all of the significant changes in energy
forms occur during the first 30 minutes of simulated time. During the
subsequent period of decay there is some rearrangement of energy due
to the field of motion, evaporation, and numerical smoothing, but it
is of minor importance.

Preceding page blank

REFERENCES

Braham, R. R., Jr., 1952: "The Water and Energy Budgets of the Thunder-
storm and Their Relation to Thunderstorm Development," *Journal of
Meteorology*, Vol. 9, No. 4, pp. 227-242.

Brown, Rodger A., 1967: "Mass and Available Energy in Growing Convec-
tive Clouds," *Journal of the Atmospheric Sciences*, Vol. 24, No. 3,
pp. 308-311.

Bunker, A. F., B. Haurwitz, J. S. Malkus, and H. Stommel, 1949: "Verti-
cal Distribution of Temperature and Humidity Over the Caribbean Sea,"
Papers in Physical Oceanography and Meteorology, Massachusetts Insti-
tute of Technology and Woods Hole Oceanographic Institute, Vol. 11,
No. 1, 82 pp.

Gates, W. L., 1972: *The January Global Climate Simulated by the Two-
Level Mintz-Arakawa Model: A Comparison with Observation*, The Rand
Corporation, R-1005-ARPA, 107 pp.

Gates, W. L., E. S. Batten, A. B. Kahle, and A. B. Nelson, 1971: *A
Documentation of the Mintz-Arakawa Two-Level Atmospheric General
Circulation Model*, The Rand Corporation, R-877-ARPA, 408 pp.

Iribarne, J. V., and W. L. Godson, 1973: *Atmospheric Thermodynamics*,
Dordrecht and Boston: D. Reidel Publishing Company, 222 pp.

Kessler, Edwin, III, 1969: "On the Distribution and Continuity of Water
Substance in Atmospheric Circulations," *Meteorological Monographs*,
Vol. 10, No. 32, 84 pp.

Malkus, Joanne Starr, 1954: "Some Results of a Trade-Cumulus Cloud
Investigation," *Journal of Meteorology*, Vol. 11, No. 3, pp. 220-237.

Murray, F. W., and L. R. Koenig, 1972: "Numerical Experiments on the
Relation Between Microphysics and Dynamics in Cumulus Convection,"
Monthly Weather Review, Vol. 100, No. 10, pp. 717-732; also, The
Rand Corporation, R-852-ARPA, 1971, 44 pp.

Ogura, Yoshimitsu, and Norman A. Phillips, 1962: "Scale Analysis of
Deep and Shallow Convection in the Atmosphere," *Journal of the Atmos-
pheric Sciences*, Vol. 19, No. 2, pp. 173-179.

Rapp, R. R., and M. Warshaw, 1974: *Some Predicted Climatic Effects of
a Simulated Sahara Lake*, The Rand Corporation, R-1415-ARPA, 31 pp.

Schlesinger, R. E., 1972: *An Investigation into the Energetics of
Severe Local Storms Using a Two-Dimensional Numerical Model*, Report
72-1, NSF Grant No. GI-31278X, Department of Meteorology, University
of Wisconsin, Madison, 54 pp.

Scorer, R. S., and F. H. Ludlam, 1953: "Bubble Theory of Penetrative Convection," *Quarterly Journal of the Royal Meteorological Society*, Vol. 79, No. 339, pp. 94-103.

Simpson, J., R. Simpson, D. A. Andrews, and M. A. Eaton, 1965: "Experimental Cumulus Dynamics," *Reviews of Geophysics*, Vol. 3, No. 3, pp. 387-431.

Spiegel, E. A., and G. Veronis, 1960: "On the Boussinesq Approximation for a Compressible Fluid," *The Astrophysical Journal*, Vol. 131, No. 2, pp. 442-447.

Van Mieghem, Jacques, 1973: *Atmospheric Energetics*, Oxford: Clarendon Press, 306 pp.